Invited Review Paper

Reflections on the university of maryland's program investigating gyro-amplifiers as potential sources for linear colliders

W. Lawson [1*], J. P. Calame [2], G. S. Nusinovich [3], and B. Hogan [4]
[1] Department of Electrical and Computer Engineering, University of Maryland, College Park, MD 20742, USA
[2] present address: Naval Research Laboratory, 4555 Overlook Ave SW, Washington, DC 20375, USA
[3] Institute for Research in Electronics and Applied Physics, University of Maryland, College Park, MD 20742, USA
[4] present address: NOAA's National Ocean Service, 1305 East West Hwy, Silver Spring, MD 20910, USA
[*] Email: lawson@ece.umd.edu

(Received January10, 2017)

Abstract: Over two decades of research on gyro-amplifiers as potential sources for linear colliders at the University of Maryland is reviewed. A 500*kV*, 400-800*A*, 1μs pulse generator energized single- and double-anode Magnetron Injection Guns to generate high-energy, small-orbit, rotating beams in a peak magnetic field over ½ T. Over 20 different gyro-amplifier configurations were tested during the course of the project. The project produced over 60 journal articles and over 100 conference presentations. Key results included 30*MW* of peak power in a second-harmonic gyroklystron operating near 19.76*GHz* and about 80*MW* of peak power with a fundamental-mode coaxial gyroklystron near 8.6*GHz*. Along the way, advances were made in the theoretical modeling of small-signal and large-signal gyroklystron performance, scattering matrix formulations of various cavity configurations, Telegraphist equation formulations of mode transducers, Magnetron Injection Gun (MIG) design, overmoded directional coupler designs, and drift tube loading. Some efforts were also undertaken to better understand the physics of beam-wave interaction in relativistic gyro-amplifiers with the goal to increase the devices' efficiency. Mostly due to problems with the final MIG, the program never achieved its goal of powering a small section for an advanced accelerator. Nonetheless, the program pushed the state-of-the-art in peak power density for microsecond accelerators, and tools developed and experience gained have positively impacted a number of gyro-amplifier devices at other institutions as well as gyro-amplifiers developed for other applications.

Keywords: Gyroklystrons, Gyro-amplifiers, MIGs, Microwave absorbers, Electromagnetic waves

doi: 10.11906/TST.001-043.2017.03.01

1. Introduction

In the mid 1980's, the Department of Energy, Division of High Energy Physics funded a program at the University of Maryland, College Park (UMD), to investigate the suitability of gyro-amplifiers as drivers for the next generation of linear colliders. The project was first led at the university by Profs. V. Granatstein, M. Reiser, and C. D. Striffler, initially with a substantial subcontract with SAIC Inc., whose effort there was led by P. Vitello, D. Chernin and A. Mondelli. All of the authors of this paper worked on the project while employed at the UMD Institute for Research in Electronics and Applied Physics.

The state-of-the-art in gyro-amplifier devices in the USA at the start of the UMD program can be seen from representative papers[1-4] to be on the order of hundreds of kilowatts at microwave frequencies. For example, a three-cavity (TE_{101} rectangular) gyroklystron at the Naval Research Lab (NRL) produced a little over 50*kW* at 4.5*GHz* with about 33% efficiency and 40*dB* gain. The state-of-the-art in high-power, microsecond amplifiers was represented by the SLAC klystrons[5], which produced 1 μs pulses of 150*MW* at 2.87*GHz* with about 51% efficiency and 59*dB* gain.

The initial plan of the UMD program was to get power levels in excess of 100*MW* in 1μs pulses at a frequency 6-7*times* higher than the SLAC frequency (of 2.856*GHz*) in four steps. The first two steps involved using right circular cavities operating in circular electric (TE_{0n}) modes to produce about 30*MW* of peak power. The initial experiments would aim for 10*GHz* using a 500*kV*, 200*A* beam that interacted with TE_{011}modes near the fundamental cyclotron frequencies[6-9]. The second tube series would aim to produce 30*MW* peak power near 20*GHz* by having the output cavity operate in the TE_{021} mode and interact resonantly with the beam near the cyclotron second-harmonic frequency. The third and fourth experiments were to utilize the same beam voltage, but with a much larger current, to produce over 100*MW* in coaxial gyroklystron circuits. Again, circular electric modes were chosen, so that the drift tubes could be cut off to all circular electric modes at the operating frequency and thereby enhance isolation between cavities for the operating mode. The initial design required 2000*A*[6], but the current was later scaled back to around 500-700*A*[8]. The third experiment output power would be near the cyclotron frequency and the final experiment output signal would be near the second harmonic.

In the following sections, we summarize the designs and advances of a number of the major subsystems of the gyro-amplifier project. We first discuss the development of scaling laws for Magnetron Injection Guns (MIGs) and then detail the design and theoretical performance of the MIGs that were developed for our experimental test bed. Afterward, we describe efforts to stabilize drift-tubes with custom and conventional lossy dielectrics. Next, we will discuss the code development done to model different high-power microwave components before presenting design and test results for key components. Afterwards, we will describe the codes developed for both small-signal stability analysis and large signal gain and efficiency determination. Subsequently, we will discuss some issues in the theory of relativistic gyro-amplifiers. In the following section, we will describe our experimental test beds before presenting our gyroklystron experimental results and comparisons with our theoretical models. Afterwards, we will describe our theoretical and experimental efforts with gyro-twystron tubes. Next, theoretical designs of depressed collectors for small-orbit gyro-amplifiers will be presented. A brief description of the impact of the GKL program on other research efforts will be given before conclusions are drawn in the final section.

2. MIG designs

Proper formation of the electron beam is crucial for efficient energy extraction of any microwave tube. In gyrotron oscillators and amplifiers operating at near cutoff frequencies, microwave power is extracted primarily from the electron kinetic energy associated with electron gyration in the external magnetic field. Hence, producing a beam with a high average perpendicular-to-parallel velocity ratio, or α, while maintaining a low axial velocity spread, is of paramount importance. The latter requirement is particularly important for longer devices, such as a gyroklystron, to enable tight bunches to be formed ballistically and maintained in the drift regions. Axial spreads significantly below 10% are typically required to achieve efficiency levels at 30% or higher.

The electron gun of choice for small-orbit beams (where no magnetic field reversal occurs so individual electron orbits do not encircle the axis) has been the Magnetron Injection Gun (MIG) [106]. Most MIGs are designed to operate with a temperature-limited (TL) thermionic cathode to maximize beam quality and have the ability to modify the total beam current. MIGs are generally one of the two largest capital expenditures and often have a long lead-time to design, fabricate, install and test. Thus, it is imperative to have the best design possible, yet the large design parameter space available can make that a formidable task.

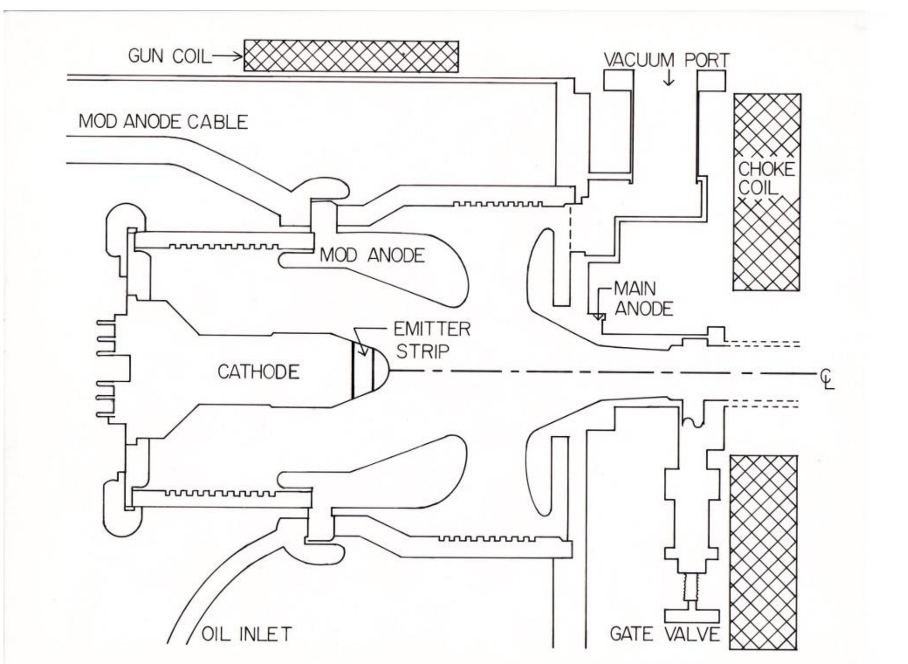

Fig. 1a The double-anode MIG used in the first two gyroklystron series at UMD.

In addition to the cathode, MIGs typically have one or two anodes. A double-anode MIG is shown in Fig. 1a. The cathode-main anode voltage determines the beam energy and the control anode helps tune the velocity ratio and beam quality. The actual cathode stalk for the double-anode

MIG for the UMD project is shown in Fig 1b. The emitter was under vacuum test at the time, so the emitter strip, which is glowing in the figure, was being heated to operating temperature.

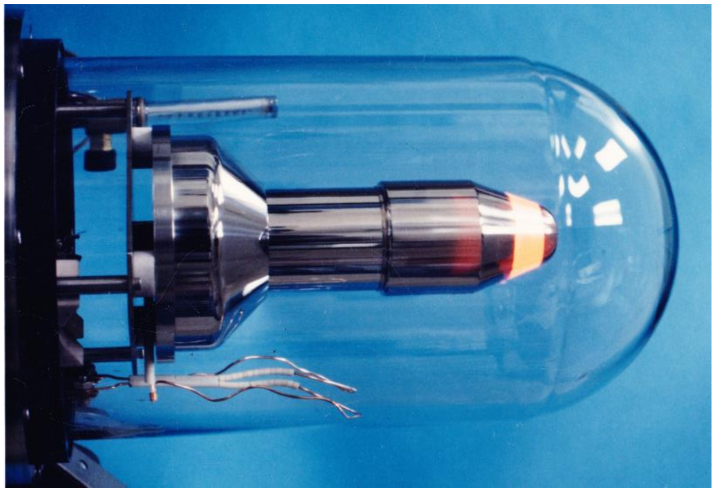

Fig. 1b The cathode stalk for the UMD double-anode MIG (emitter is heated).

A single-anode MIG is shown in Fig. 2a and the actual emitter assembly for the UMD single-anode MIG is shown in Fig. 2b. The lack of a separate control anode removes one knob that can be used to adjust the velocity ratio, so accurate MIG design and simulation is even more important than with a double-anode MIG. For both configurations, the magnetic field profile can also be used to affect velocity ratio changes. The single-anode MIG does have the advantage of a simpler design, so both the MIG and the pulsed power source can potentially be more compact and less expensive.

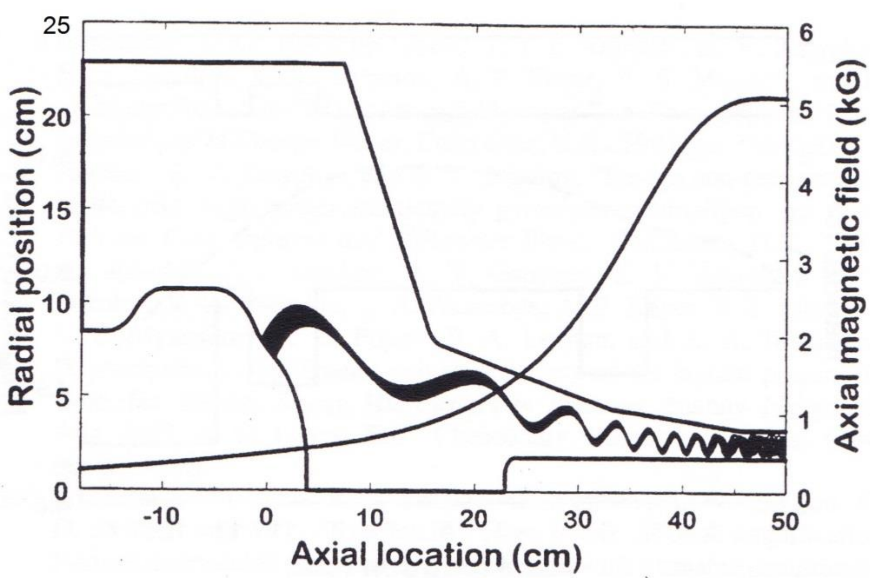

Fig. 2a The single-anode MIG used in the coaxial gyroklystron series at UMD along with simulated beam trajectory and nominal axial magnetic field profile. Taken from Ref. [8].

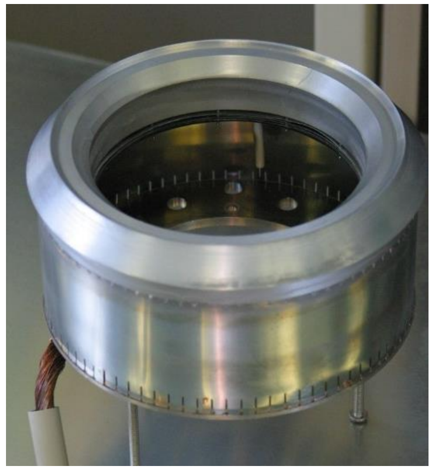

Fig. 2b The emitter assembly for the UMD single-anode MIG.

The majority of the MIG work on the GKL project involved temperature-limited guns. At the beginning of the project, Prof. Mark Baird was developing a set of analytic "trade-off" equations[10] for MIG designs that could be used to substantially narrow the design space and quickly arrive at preliminary design geometries that would subsequently be modified with computer simulation [11-12]. The UMD team worked with Prof. Baird to finalize and test these equations.

There are seven trade-off equations based on physical principles and adiabatic approximations. For a double-anode MIG, the MIG parameters that are calculated are the required magnetic compression (ratio of the axial magnetic field in the microwave circuit to the field at the cathode), cathode slant length, anode-cathode gap, and the intermediate anode voltage. The equations will also estimate the relative cathode loading (as compared to the space-charge limit), peak electric field at cathode, and guiding center spread. To calculate those values, one needs to input beam parameters required by the microwave interaction: beam power, beam voltage, magnetic field in circuit, average guiding center radius, and velocity ratio. Four more parameters are required by the trade-off formalism. Typically, we focus on cathode parameters: average cathode radius, cathode slope, actual cathode loading and the distance from the anode to cathode in Larmor radii. These equations are quite flexible; for example, one could define the guiding center spread and calculate the required cathode loading instead. The trade-off equations depend heavily on the cylindricity parameter, μ, which under adiabatic conditions is the ratio of the Larmor radius at the cathode to the average cathode radius. A typical application of the equations could be to set limits on the maximum acceptable values of peak electric field, relative current density, and maximum beam radius and then vary the free cathode parameters to find the parameter space where all boundary limits are satisfied. If there is a considerable viable range of parameters initially, further restrictions (like limiting the magnetic compression) can be considered. If there is no viable parameter space, it may be necessary to re-think fundamental beam parameters or try an alternative MIG geometry (like a single-anode MIG or vice-versa).

These trade-off equations were used to find a starting point for all of our MIG designs. As an example, our first MIG was a double-anode design[13]. The desired beam parameters are summarized in Table I. One design goal was to keep the cathode electric field below 60*kV/cm*, so that the peak electric field anywhere in the MIG (typically at the cathode nose) would be less than 120*kV/cm*. Another design goal was to keep the cathode loading below 30% of the space-charge limit (SCL), in order to minimize the needed cathode temperature and minimize SCL loading effects[14]. A viable design was found for the electrode specifications collected in Table II. Computer simulations were used to determine the exact MIG geometry. The principle variables adjusted during the simulation process included the diameter of the cathode stalk, the length of the magnetic compression region, the length of the control anode, the distance between anodes, and the shape of the main anode in the adiabatic compression region. The final simulation design was shown in Fig. 1, and some key MIG parameters and simulated results are listed in Table III. The simulations showed that we would be able to produce a high-quality beam with all the necessary parameters to achieve the goals for our first two gyroklystron series. While velocity spread was never measured experimentally, our microwave results for those tubes (as well as experimental measurements of α) were consistent with the simulated MIG results.

Tab. I The desired beam parameters for the first gyroklystron tubes.

Beam power (*MW*)	80
Beam voltage (*kV*)	500
Beam current (*A*)	160
Guiding center radius (*mm*)	7.85
Maximum beam location (*mm*)	13.5
Velocity ratio α	1.5
Axial velocity spread (%)	<10
Circuit axial magnetic field (*kG*)	5.65

Tab. II The electrode specifications for the double-anode MIG.

Cathode radius (*mm*)	22.8
Cathode slant length (*mm*)	20.0
Cathode slope (°)	20
Cathode - control anode gap (*mm*)	61.3
Cathode – main anode gap (*mm*)	55.0
Control anode voltage (*kV*)	143
Cathode loading (A/cm^2)	5.61
Magnetic compression ratio	12

Tab. III The simulated double-anode MIG results

Average velocity ratio	1.52
Axial velocity spread (%) at 160 *A*	5.6
Average guiding center radius (*mm*)	7.81
Maximum beam location (*mm*)	12.5
Peak cathode field (*kV/cm*)	91
Peak anode field (*kV/cm*)	84
Average cathode field (*kV/cm*)	52

Our final two gyroklystron series required a much larger beam current and, subsequently, a much larger guiding center radius. We considered both double-anode and single-anode MIG designs[15]. The double-anode design had a smaller cathode slant angle, resulting in superior guiding center spread. There was also a larger viable design space. However, the single anode design had a more compact geometry and could operate over a wider range of beam currents with low velocity spread. The simulated velocity spread of the single-anode design (6.1%) was superior to the best result for the double-anode MIG (7.5%). The double-anode MIG had lower peak electric fields (by about 8%) and lower cathode loading (by about 90%). The single-anode design was selected for fabrication due to the compact design and better velocity spread. In retrospect, our single-anode MIGs suffered from non-uniform current density and vacuum issues, and so double-anode MIGs may have been a better design choice.

A number of other MIG studies were performed that did not result in actual hardware fabrication. We looked at the scaling laws of each trade-off equation for operating frequency, beam voltage, peak electric field and cylindricity[16]. For example, the peak beam power available for a microwave device from a MIG is proportional to the peak electric field and inversely proportional to the operating frequency. This latter dependence, rather than an inverse-squared dependence on frequency, along with the ability to use overmoded cavities, gives gyroklystrons a significant advantage over klystrons and other amplifiers at high frequencies. Computer simulations were performed for a select number of scaling scenarios to demonstrate the ability to quickly scale an existing design to new design with one major parameter change (e.g. taking a MIG designed for a 10*GHz* gyroklystron and generating a MIG design for a 30*GHz* gyroklystron).

Furthermore, we investigated the suitability of developing space-charge-limited MIGs. In the first paper, we designed an SCL alternative to our 500*kV*, 500-600*A* TL MIG for our coaxial gyroklystron series[17]. Both the TL and SCL designs yielded similar values for beam quality (an axial velocity spread under 7%) at an average perpendicular-to-parallel velocity ratio of 1.5. The peak electric field was 7% higher for the SCL design and the average cathode loading (7.6A/cm^2) was about 27% higher than for the TL design. The motivation for this study was that, for the TL design, realistic variations in emitter temperature or work function translated into azimuthal current variations that hindered the operation of the device. The SCL design should have had a quite uniform azimuthal distribution of cathode loading and, therefore, should have been a better electron beam source for many high-power gyrotrons. A disadvantage of the SCL design is that the experiment could only modify the current by changing the beam voltage as well. To overcome this limitation, the second paper explored using non-intercepting control anodes near the emitter strip to adjust beam current[18]. Two designs were developed and simulated. Both designs were developed with the basic goal of achieving a 500*kV*, 500*A* beam for the gyroklystron experiment in our laboratory. The first design had small electrodes that could be adjusted by +/-2% of the main beam voltage to adjust the current by +/-60%. The second design had larger control electrodes that could be biased sufficiently to cut off the beam flow even when the full beam voltage is applied. High quality beams (under 6% axial velocity spread) were achieved in simulations over a range from 200 to 800*A*. Peak electric fields did get significant at some control voltage levels (up to 135*kV/cm*), and cathode temperature would have to be significantly higher than that for a thermionic design, but overall the study seemed to indicate that an SCL MIG might have been the best choice for our MIG for the coaxial gyroklystrons.

Finally, we collaborated on the design of an inverted MIG for the coaxial gyroklystrons[19], which had excellent simulation results and the added benefit of high rep-rate operation by avoiding small pins in the drift regions to support the inner conductor. Neither the inverted MIG nor the SCL MIGs were ever built.

3. Development of tools and techniques to stabilize drift-regions

A key challenge in the UMD gyroklystron program involved the prevention of spurious electromagnetic oscillations (instabilities) in the drift tubes between cavities, as well as in the conical-walled beam tunnel in the magnetic compression region between the MIG and the gyroklystron input cavity (MIG downtaper). Such oscillations, if allowed to proceed unabated, have a variety of deleterious effects. These effects ranged from reductions in spectral purity that could affect the phasing of multiple amplifiers for the intended accelerator application, to a significant reduction in output power and efficiency in the amplifier operating mode (by interfering with the carefully orchestrated beam bunching, or by exacerbating velocity spread). At worst, unintended oscillations can lead to the complete disruption of the beam with associated beam interception on the vacuum walls, leading to damage from heating, outgassing, and electrical breakdown. The problem of oscillations was particularly challenging in the UMD program due to the overmoded cavities and beam tunnels, the use of which was necessary to accommodate the electron beam needed to meet the amplifier output power requirements. In the first UMD ~10*GHz* devices, which used TE_{011} circular electric modes in the cavities, the Larmor radius of the beam plus allowances for beam optics non-idealities resulted in larger drift tube radii, which, although properly cutoff to the TE_{01} mode at the operating frequency, were not cutoff to the lower-order TE_{11}, TE_{21}, and TM_{01} modes in a range of frequencies over which unintended beam-wave interactions could occur [7].

It became clear through early cold-tests that conventional textbook schemes for loading non-TE_{0m} modes, such as a tightly wound helical wire backed by a microwave absorbing ceramic, provided grossly inadequate attenuations per unit length. Emphasis shifted towards the use of drift tubes consisting of alternating ceramic and metal rings, which was a configuration previously employed by many research groups for the beam tunnel upstream of the cavity in gyrotron oscillators. In this general geometry, resonant trap configurations with a relatively low-loss MgO-SiC ceramic and non-resonant configurations with a highly lossy BeO-SiC absorbing material were investigated in the drift tubes, while the downtaper in both cases used a similar non-resonant geometry with aluminosilicate-carbon composite[20] absorber rings alternating with metal rings. Early two-cavity gyroklystron hot-test experiments at UMD using these schemes were performed, but severe oscillations in the drift tube and downtaper regions were noted[21]. Experimentally it was possible to diagnose the frequencies and mode structures, with the majority of the instabilities found to be TE_{11}-like at frequencies of 6-8.5*GHz* (all non-axisymmetric modes in dielectric-lined or non-uniform wall cylindrical waveguiding structures are actually hybrid modes, but the character of these particular modes is primarily TE). The main problem was the relatively narrow axial dimension of the lossy ceramic rings, and the relatively small total areal percentage of the drift tubes/beam tunnels occupied by the lossy material. The narrow rings simply did not admit enough azimuthal electric field (and axial H-field) to allow the necessary radial power flow into the absorber, and the relatively low percentage coverage (< 50%) further limited the total attenuation.

Prior to the UMD program, the conventional wisdom in gyro-devices (and in vacuum electronics in general) was to use as little lossy dielectric as possible in the drift tubes and beam tunnels and to employ it in more of a perturbative manner, so that the propagation characteristics and transverse field profiles in the loaded structures would closely resemble metal waveguide, albeit with the intended losses. The motivations for this philosophy were numerous, but they were based mainly on concerns about beam interception onto the ceramics, with the idea that keeping most of the surface area metal, and even recessing the inner radii of the ceramic so that the metal rings could act as beam scrapers, would prevent problems. Another motivation for the traditional sparse use of ceramics involved the desire to rigorously maintain cutoff to the operating mode; it was feared that dramatic reductions in metal and replacing it with ceramic might allow propagation and permit feedback oscillations between cavities (via the TE_{01}-mode in this case). Large amounts of dielectric were also viewed as potentially harming the electrostatic stability of the electron beam propagation. It became clear from early experiments in the UMD program that this conventional wisdom needed to be radically changed if the program was to succeed, and that lossy dielectrics would need to occupy the majority of the surface area in large, contiguous regions within the drift tubes and beam downtaper. Metal would primarily be reserved for the highest field regions within and immediately adjacent to the cavities, and of course, in the entire high power output waveguide/beam dump region beyond the output cavity.

Subsequent cold test experimentation examined drift tubes consisting of long lengths of absorbing material made up of adjacent ceramic (BeO-SiC) rings with tapered inner radii, to produce a sawtooth-like axial profile of ceramic lining, with metal only at the far ends. The sawtooth profile was investigated with the idea of reducing radial electromagnetic reflections between the high dielectric constant ceramic and vacuum. Dramatically higher attenuations were obtained compared to the conventional narrow ceramic/metal ring configuration, although at first, the experimentation was empirically-driven. Around this same time period, however, dramatic improvements were made in the modeling and simulation capability within the UMD gyro-amplifier program, with the creation of scattering-matrix codes that could handle junctions between lossy dielectric-lined cylindrical waveguide. This capability was married with UMD codes used to predict start oscillation currents, and together, the first detailed look at the structure of the instabilities became available. In addition to more localized pure drift tube modes, it was clear than spatially extensive, “whole tube” instability modes with TE_{11}-like character existed in the gyroklystron, with frequencies consistent with early hot-test experimentation. These whole tube modes ('global modes') have axial field profiles that encompass all the drift tubes and cavities, since at these lower frequencies, the cavities act mostly like additional metal sections and do not serve to break up the axial field profile. Accordingly, the long interaction length leads to very low start oscillation currents, which made the need for effective dielectric loading covering the majority of the interaction circuit apparent. The new modeling capability was combined with the cold test investigations to confirm that the mostly-ceramic drift tube configuration would provide the needed stability to the TE_{11}-like whole tube modes (and TE_{21}-like modes as well). Equally important, the selected configuration was shown both in cold test and through modeling to provide sufficient attenuation to the TE_{01} mode to provide inter-cavity isolation and prevent oscillations in the operating mode.

One area that proved particularly challenging was the downtaper region. The problem here was that the radius of the taper was changing, and since it was in the magnetic compression region, the magnetic field was also changing. Hence, three things were varying at the same time, namely the cyclotron frequency, the beam perpendicular-to-parallel velocity ratio, and the cutoff frequency of the electromagnetic waves supported by the structure. Accordingly, some sort of instability could occur just about anywhere in the downtaper region, since there was likely to be a robust cyclotron maser interaction at some fortuitous point, and that location and frequency would change as the device operating parameters were varied. Furthermore, disturbances in the electron beam optics due to instabilities were particularly harmful in this compression region, since any associated disturbances the velocity distribution got exacerbated as the beam was compressed, often to the point of wall interception and sometimes undergoing magnetic mirror-like reflections. The realization of this fact, and hot test results showing very persistent, tunable instabilities in the downtaper, required a very robustly attenuating, broadband dielectric loading scheme. The complexity of the geometry and the spatially-varying interaction made a detailed theoretical treatment prohibitive at that time, although a target attenuation per unit length was roughly estimated. Lacking a detailed analysis, an experimental approach was taken involving covering essentially the entire downtaper with aluminosilicate-carbon lossy ceramic in a series of stepped radial segments, and using only the smallest amount of metal possible, mainly to secure the lossy materials into position and provide a very limited shielding at the steps from stray electrons.

Extensive hot tests of a sequence of two-cavity gyroklystrons proved the viability of the new dielectric loading concepts. Each iteration of the loading structure provided an additional margin of stability, first allowing significant gain and 2-3*MW* of output power[21]. With further improvements in stability and, most importantly, the incorporation of magnetic field tapering to optimize cavity detuning, 24*MW* of amplified power at high gain was achieved in the TE_{01} mode at ~ 10*GHz*, with the complete absence of spurious oscillations regardless of input power (i.e., zero-drive stable)[22, 23]. The work was extended to a three-cavity device with further advancements in the drift tube loading technology and analysis[24]. Subsequent work in the UMD program with the harmonic gyroklystrons operating at ~20*GHz* in the TE_{02} mode used many of the same drift tube dielectric loading schemes as the fundamental harmonic device, and they were similarly successful[25, 26]. In addition to controlling all fundamental harmonic instabilities, there was the additional issue of preventing rearwards radiation at the second harmonic backwards from the output cavity towards the input cavity and the gun, since the TE_{02} mode can partially convert to TE_{01} at 20*GHz*, which would not be cutoff by the drift tube size. By this time, the UMD theoretical tools had advanced sufficiently to allow this issue to be preemptively avoided by proper design, and as a result, it never manifested itself experimentally. A combination of a tapered radius (with nonlinear spatial profile) on the upstream side of the output cavity, to minimize TE_{02} to TE_{01} mode conversion, and a resonant lossy-dielectric-loaded trap immediately upstream of the output cavity, was employed.

The higher-powered UMD coaxial gyroklystrons at ~8.6*GHz* provided additional challenges to stability. With the larger coaxial geometry, the number of potentially unstable modes was significantly increased since many modes with nonzero azimuthal indices were supported by the structure, each of these with various radial indices. Vigorous beam-wave interactions could occur at multiple cyclotron harmonics as well. All of these features had to be accounted for during the design process. By this time, the improved theoretical understanding and computational tools developed in the UMD program were utilized up-front during the design process. The coaxial drift tube loading scheme that was adopted involved lossy dielectrics on both the inner and outer conductors. The outer conductor in the drift tube areas had concentric layers of two different dielectrics (one BeO-SiC, the other aluminosilicate-carbon), since it was determined through modeling studies that a single layer of one composition could not properly load enough modes. By proper choice of the thicknesses of the materials, and carefully taking account the frequency-dependence of the dielectric properties of each materials, the loading structure was optimized to provide wideband and multi-mode loading. Essentially, at some frequencies and for certain modes the two concentric liners work together to provide loading, while under other conditions, only one of the two liners does the bulk of the work. However, using just the outer conductor loading scheme was found (through modeling) to not be sufficient to properly load all modes. Accordingly, the inner conductor in the drift tube sections was covered with axially alternating rings of the two different compositions of lossy ceramic, with one material making up for the poor performance of the other in a complementary fashion. Unfortunately, it was not possible at the time to devise a similarly complicated and optimized loading scheme for the downtaper, in part due to a lack of theoretical tools at the time to handle the more complex problem of spatially varying geometry and magnetic field, and also due to mechanical constraints of the vacuum envelope. The downtaper inner and outer conductors were simply covered with aluminosilicate-carbon absorbing ceramics, with much of the thickness and placement dictated by mechanical constraints. Overall, the downtaper proved to be acceptably stable against most oscillations, especially considering the immense beam power used in the coaxial gyroklystron. The gyroklystron produced about 80*MW* of output power at ~ 8.6*GHz*[27, 28], proving the effectiveness of the drift tube and downtaper loading schemes. However, there remained some unsolved problems in reaching the full design capabilities of the MIG (current and beam velocity ratio), some of which might have been due to hidden stability problems in the downtaper area.

Looking back on these gyro-amplifiers in the UMD program, one can see that the conventional wisdom that existed in the mid-1980s against the massive incorporation of lossy dielectrics into gyro-amplifiers suffered from some conceptual biases that turned out to be less important in practice. Regarding beam interception and charging, the problems are not nearly as severe with lossy composites based on silicon carbide (such as BeO-SiC) as with pure insulating ceramics like SiO_2, Al_2O_3, or BeO. Although BeO-SiC at the 20-40% SiC content is an insulator at low electric fields, under high energy electron impact and locally high electric fields, there is a large conductivity within the SiC phase itself, and considerable SiC grain-to-grain hopping and tunneling conductivity between grains in these nearly-percolating systems that helps drain away a modest amount of spurious beam interception. This is particularly true in pulsed devices like the UMD gyroklystrons and any similar devices for the high peak power accelerator application. Similarly, the aluminosilicate-carbon dielectrics used in various regions actually has an inherent conductivity, since the carbon phase is completely percolating, although one still must keep interception very small to avoid heating and outgassing. Hence, it is possible to use a large surface area of lossy dielectric at the expense of metal, provided the beam optics are well-designed and the device is well-aligned, and with proper choice of dielectric materials. With regards to concerns about inadvertently reducing the attenuation to the operating mode with extensive dielectric, this proved to not be a significant problem. With careful design, it was possible to select the lossy dielectric geometry and materials properties (via composition selection) in a way that provides attenuations comparable to cutoff waveguides of the same inner radius. In fact, it was found during the UMD program that one can design the drift tube absorber structure to radially expel the fields of the operating mode from the dielectric, making the structure behave much like a (cutoff) metal waveguide, while at the same time drawing the fields of the spurious modes radially outwards into the dielectric, which provides both heavy losses and grossly decreases the beam-wave coupling in the vacuum region. As for the conjectured possibility of gross disruptions of the beam electrostatic stability and propagation by the presence of dielectric liners, at least for the types of dielectrics and geometries used in the UMD problem, this issue did not seem to occur to a measureable extent. Finally, the extreme flexibility afforded by dielectric-dominated loading schemes, especially those involving multiple dielectric materials (including their inherent frequency responses) and multiple loaded surfaces (as in coaxial devices), can be used to great advantage to simultaneously prevent dozens of potential instabilities. This demonstrated capability and flexibility of lossy dielectric loading was never envisioned during the initial stages of the UMD gyro-amplifiers program, but it is a significant achievement of the program that will continue to be useful in many different types of vacuum electronic devices and other high power microwave applications.

4. High power microwave component design

In order to manipulate the microwave power produced by the gyroklystrons and evaluate the performance of the tubes, a number of high power microwave components had to be designed, fabricated and tested. For example, multiple diagnostics were used to evaluate peak power. An anechoic chamber was designed and built that could remotely sweep out from the tube centerline to estimate output mode and power. A liquid calorimeter measured average output power. Directional couplers were developed for extremely overmoded waveguides[29, 30]. To avoid excessive electric fields in the anechoic chamber, the circular output waveguide had a diameter of 12.7*cm*. Near 10*GHz*, over two dozen modes can exist in that waveguide, so the selection of coupling apertures became complicated. The circular guide served as the main arm of the coupler and the narrow wall of standard rectangular waveguide served as the secondary arm. Since the secondary arm was not as overmoded as the main arm, the phase velocities of the desired coupled mode could not be matched in the two arms.

The four main constraints for the directional coupler design were that (1) the nominal coupling of the desired mode in the forward direction needed to be about -60*dB*, (2) coupling of any potentially unstable mode had to be less than -60*dB* at the expected oscillation frequency, (3) coupling of all modes in the main line had to be less than -60*dB* at the nominal operating frequency of the gyroklystron and (4) the reverse coupling of the operating mode had to be suppressed by at least 20*dB*. Coupling holes were always made in pairs to suppress reverse coupling of the operating mode, but the pair spacing was not always uniform. With a systematic variation in these spacings, along with code developed to look at all relevant modes, compact (0.7*m* or shorter) designs were made that met all of the design criteria. The couplers were fabricated and measured performance was found to be in good agreement with the analytic code predictions[30], so the couplers were able to be a valuable tool for peak power measurements.

Right circular and coaxial tapers for the output waveguide were also critical components for the gyroklystron devices. These tapers needed to transform the waveguide from the radius needed for efficient output cavity operation to the radius needed for the anechoic chamber connection with as little mode conversion and reflection as possible. In addition, for the coaxial gyroklystrons, the taper needed to eliminate the inner conductor.

The design of circular waveguide tapers was relatively straightforward. A code based on Telegraphist's equations was written and standard tapers (e.g. linear, raised cosine and Dolph-Chebyshev) were evaluated against the design criteria[31]. Since the taper was overmoded, numerical instabilities arose at radii that corresponded to cutoff radii for a specific frequency. The code was stabilized by assuming an appropriate loss for the conducting wall. Taper simulations from the Telegraphist's code were checked by comparing the results to that of a scattering-matrix formulation[32]. Results were always found to be in excellent agreement.

The early gyroklystron experiments actually required two uptapers – one to transition from the output cavity to the beam dump section and a second to transition from the beam dump to the anechoic chamber diameter (the output waveguide is shown in Fig. 3). For the circular guide, the smaller taper was best served by a Dolph-Chebyshev taper and was fairly broadband. For example, for the operating TE_{01} mode, mode conversion and reflection was well below -55*dB* from 9 to 11*GHz* and below -40*dB* from 8 to nearly 12*GHz*. For the large circular uptaper, a raised cosine gave the best result for mode conversion of the operating mode, but over a much narrower bandwidth. Still, mode conversion to other TE_{0n} modes was less than -45*dB* and the TE_{01} reflection was less than -60*dB* near the operating point.

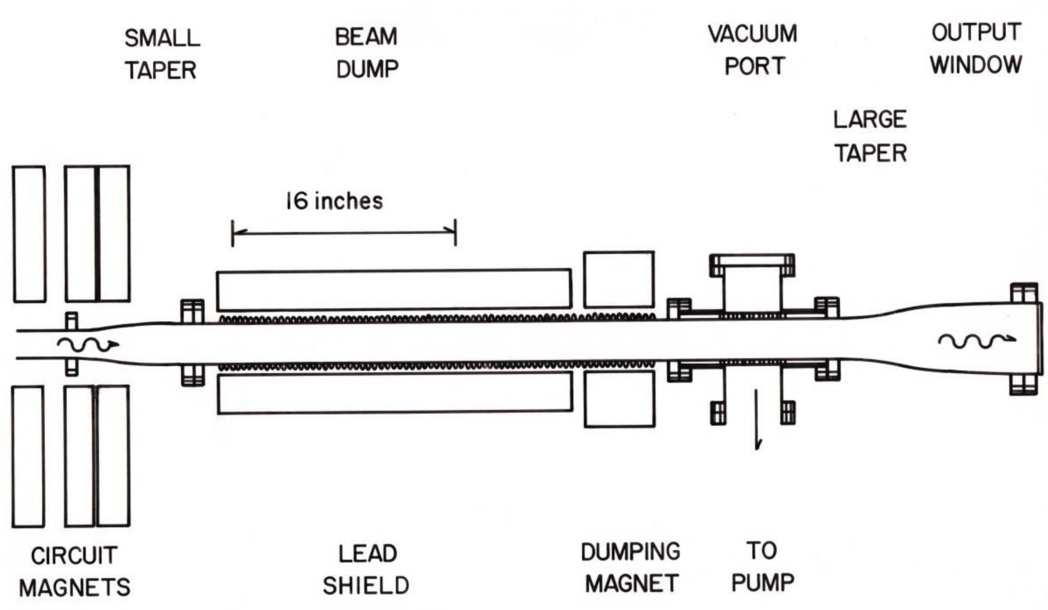

Fig. 3 The output waveguide for the first two gyroklystron series

The design technique was also extended to include systems that were coaxial for a least a part of the transition[33]. The Telegraphists' results for the coaxial case were also checked against a scattering matrix formulation for coaxial systems[34]. Once again, agreement was always excellent for the two approaches, lending considerable confidence to the results. Because of the larger guiding center radius, our coaxial gyroklystron needed only one non-linear uptaper. That component was realized by placing a linear downtaper on the inner conductor (until the inner radius went to zero) and a modified Dolph-Chebyshev taper on the outer radius. For our second-harmonic coaxial gyroklystron, the output mode was the TE_{02} and mode conversion to the TE_{01} and TE_{03} modes were potential problems. The optimized design had mode conversion of less than -30*dB* for either mode over a 2*GHz* band centered at the output frequency (17.14*GHz* in this case). At the output frequency, TE_{03} mode conversion was below -35*dB* and TE_{01} mode conversion was below -45*dB*. Overall, these two types of codes for cold structures allowed us to efficiently design compact tapers for circular and coaxial systems that led to very pure output modes for the amplified microwave signals.

A number of mode converters were designed, built and tested during the GKL project with an idea that we would need them to feed power into an accelerator structure[35-37]. First, symmetric, ripple-wall converters were designed to convert microwaves from harmonic systems (e.g. TE_{03} or

TE_{02} modes into the TE_{01} mode)[35, 107]. Both analytic codes described above were used in the designs. Nonlinear Dolph-Chebyshev tapers were integrated into the designs. Our design goal was to have over 99.9% mode conversion at the operating frequency in a compact design with a 1% bandwidth of several hundred *MHz*. For a TE_{02} to TE_{01} converter, a simple constant-ripple converter with 6 stages was adequate. For a TE_{03} to TE_{02} mode converter it was necessary to have a non-constant ripple amplitude to meet the design requirements. All designs were fabricated and tested and there was excellent agreement between theory and experiment for all cases.

The Telegraphist's code was modified to analyze serpentine converters, again for potential interaction with an accelerator section[36]. The code was used to design a TE_{01} to TE_{12} mode converter and a TE_{11} to TM_{01} mode converter. The second design was done as a reference and achieved a 99.99% conversion theoretically. (The scattering-matrix code could not be used as a check for these designs.) The first component had a potential application for our gyroklystron and the design realized a 98.5% conversion. This mode converter was built and experimental results were consistent with the theoretical predictions.

The final high-power structure designed and tested for the accelerator application was a compact TE_{01} (circular) to TE_{20} (rectangular) mode converter[37]. The TE_{20} mode was later split into two TE_{10} rectangular guides to be fed into an accelerator structure. This was our only microwave component besides the input cavity of our gyroklystron circuit that was not designed by a code developed at the University of Maryland. Instead, the code Maxwell 3D was used to realize the design[38]. The design goals included having a power balance between the two output arms of about 0.15*dB* over a 200*MHz* band and a phase balance of about 3-4 degrees. A low power version of the device was fabricated and tested and the experimental results were consistent with the design. While none of the mode converters was ever interfaced between the GKL output and the accelerator input, all converters appeared to be suitable for the application.

5. Theoretical gyroklystron circuit design

During the more than two decades of the GKL project, gyroklystron tubes were designed from 8.5*GHz* to 95*GHz*[7, 39-50]. Most, but not all, of the designs were for accelerator applications. Only designs from 8.5*GHz* to 20*GHz* were realized in the laboratory. Many codes were utilized to design the entire system. Codes to design the MIG, the magnetic field, and high power microwave components are described elsewhere in this paper. We define the microwave circuit to be the part of the tube after the MIG downtaper and up to the start of the beam dump – the region where significant beam-microwave interaction is expected to occur. There were three main codes that were developed at UMD and used in the design process for the microwave circuits. Commercial codes to verify designs or handle non-symmetric geometries were used sparingly[82, 83].

The first code utilized was the scattering matrix (SM) code (with whichever version was needed for the geometry of a specific tube)[32, 34]. Except for the input cavity coupler, the circuits were axisymmetric, normally with abrupt changes to the circular or coaxial waveguide radii. That geometry was well suited for the scattering matrix code. Second harmonic right circular cavities and the initial uptaper had continuously-varying radii, but those sections were approximated by 10-30 discrete steps. The SM code calculates the cold-cavity fields in each region, as needed for the small-signal and large-signal codes described below.

Linear stability for each individual cavity was calculated with the small-signal code called QPB [7]. This code took the results of the SM code for any resonance calculated, and calculated the threshold for instability as a product of the cavity quality factor (Q) and the nominal beam power (PB). The threshold quantity was calculated as a function of a constant magnetic field, average velocity ratio and other beam parameters. If a good estimate of the Q for that mode was known, dividing the Q and the beam voltage out, we calculated the start current for that resonance.

The large-signal code, known as MAGYKL (for MAryland GYroKLystron) used the SM cold-cavity fields for the entire circuit to estimate the efficiency of the tube[7, 39]. This code also required information on the input power, cavity quality factors and resonant frequencies, and the axial magnetic field profile.

Details of the code techniques are given in the reference papers. Design of a microwave tube was an iterative process. First, the SM codes were used to getting a starting point for the tube geometry. QPB was then used to see if the cavities were individually stable for the expected beam current and anticipated magnetic field. Finally, MAGYKL was used to optimize the beam-microwave efficiency. While maximizing tube performance, magnetic field profile, quality factors, and drift tube lengths, etc. were often modified. The SM codes were then used to modify the geometry, and QPB was used to evaluate stability of the modified design. MAGYKL would then attempt to verify large-signal performance with the modified geometry. This iterative process was repeated until the design converged to what we believed was a viable, optimal design.

Specific design results for tubes that were realized are presented later in this paper. The codes described here for the design process were also used to analyze performance once the actual experimental parameters of a given tube were known, Comparisons of theoretical modeling and experimental measurements are also given in that later section.

6. Some Issues in the Theory of Relativistic Gyro-Amplifiers

This section is restricted by discussion of some physical effects important for operation of relativistic gyro-amplifiers that were analyzed in the framework of a given program. These issues include: first, the frequency multiplication in a multi-stage gyro-amplifiers in which the frequency doubling takes place in each successive stage operating at the doubled cyclotron harmonic resonance, viz., for example, in the three-cavity GKL the sequence of resonant harmonics is 1-2-4. Second, the interaction with forward waves (e.g., in gyro-twystrons) allows one to increase the amount of the kinetic energy associated with the axial electron motion that can be withdrawn from an electron beam in the process of beam-wave interaction. Lastly, in the devices with prolonged interaction in the output stage, first, electrons can be prebunched after initial modulation and then, this bunch can be trapped by a wave and gradually decelerated in a tapered external magnetic field. Below, all these issues are briefly considered.

Harmonic multiplication.

In the second harmonic gyroklystrons and gyro-twystrons mentioned above, the input section operated at the fundamental cyclotron resonance, while the output section operated at the second cyclotron harmonic. So the frequency doubling took place in such devices. It was attractive for further frequency increase to add one more output section operating at the fourth harmonic, thus doubling the output radiation frequency at a given external magnetic field. In the process of analyzing such devices with successive frequency doubling some general features in electron ballistic bunching were found[53]. First results of the code simulations for a 1-2-4 device were presented in Ref.[40]. It was shown that in a GKL having the same first two (input and buncher cavities) as in a previously designed three-cavity, 1-2-2 device, the efficiency of the 1-2-4 device with the 34.27*GHz* output can reach16% in the absence of electron velocity spread. In a 4-cavity, 1-2-4-2 device, where, as in linear-beam klystrons, the penultimate cavity operates at a higher harmonic for efficiency enhancement, the efficiency can exceed 54%[54].

Relativistic gyro-amplifiers with forward waves

As mentioned above, many gyro-devices (including the most ubiquitous gyrotron oscillators) operate near cutoff. Therefore, in the cyclotron resonance condition

$$\omega - k_z v_z \approx s\Omega \tag{1}$$

between the Doppler-shifted wave frequency (ω and k_z are the wave frequency and the axial wavenumber, respectively) and the resonant harmonic of the electron cyclotron frequency Ω the Doppler term $k_z v_z$ (v_z is the electron axial velocity) plays a negligible role ($k_z << \omega / c$ near cutoff). This fact makes the device operation relatively insensitive to the axial velocity spread. At the same time, however, only the kinetic energy associated with electron gyration can be transformed into the energy of microwave radiation. So there was a challenge to figure out when and to what extent one can benefit from operating with forward waves allowing, in addition to the transverse interaction, also to extract the energy from axial motion. Some experimental observations [24] indicated that this could be possible.

The first theoretical study was performed in[55] where it was shown that the efficiency of the gyro-twystron operating at the fundamental cyclotron resonance could reach 47%, while at the second cyclotron harmonic the 35% efficiency can be achieved. That analysis was based on using the so-called *auto-resonant effect*. The effect of the *autoresonance* was discovered in 1963 [56, 57]. It was shown in these papers that, when the wave propagates along the magnetic field with the phase velocity equal to the speed of light ($v_{ph} = \omega / k_z = c$), the changes in the Doppler term caused by the changes in electron energy, exactly compensate the changes in the electron cyclotron frequency in (1). Therefore, under such conditions, if the cyclotron resonance condition is fulfilled at the entrance to the interaction space, the electrons will stay in resonance with the wave no matter how greatly the electron energy is varied in the process of interaction. Later, it was shown [58] that for providing coherent electromagnetic radiation from relativistic electrons it makes sense to create conditions close to the cyclotron autoresonance, but having the Doppler-shifted wave frequency not exactly equal to the electron cyclotron frequency (or its harmonic). Then, a small difference between the changes in the Doppler-shifted wave frequency and the cyclotron frequency may lead to gradual phase bunching of electrons (this phase bunching can be characterized as $\theta = \int_0^\tau \left(\omega - k_z v_z\left(\mathrm{E}\right) - s\Omega\left(\mathrm{E}\right)\right) dt'$) and, then, electron bunches can be decelerated by the wave of a reasonably small amplitude (below the breakdown limit) and the coherent EM radiation may take place. The device utilizing this sort of operation was called the <u>c</u>yclotron <u>a</u>uto-<u>r</u>esonance <u>m</u>aser (CARM). Corresponding processes were analyzed in[59]. That analysis (as well as the one used in[55]) was based on the relation between the changes in the electron energy E and axial momentum p_z in the process of interaction with the plane EM wave derived in[56, 57]

$$E - v_{ph} p_z = const. \tag{2}$$

Equation (2), known as the *autoresonance integral*, being taken together with the classical relation between the electron energy and momentum allows one to determine the condition for complete deceleration of electrons. This condition can be given as the optimal wave phase velocity (normalized to the speed of light, $\beta_{ph} = v_{ph} / c$), allowing for both orbital and axial components of the electron momentum become equal to zero simultaneously. This optimal phase velocity can be defined as the function of the initial electron energy (normalized to the rest energy, $\gamma_0 = \mathrm{E}_0 / m_0 c^2$) and initial electron orbital-to-axial velocity ratio ($\alpha_0 = v_{\perp 0} / v_{z0}$):

$$\beta_{ph,opt} = \left[\frac{\left(1+\alpha_0^2\right)\left(\gamma_0 - 1\right)}{\gamma_0 + 1}\right]^{1/2}. \tag{3}$$

Equation (3) allows us to readily find out [60] when one can withdraw all electron kinetic energy in the process of interaction with fast waves ($\beta_{ph,opt} > 1$) and, alternatively, when it can be done with slow waves ($\beta_{ph,opt} < 1$). As follows from (3), the interaction of electrons with fast waves is optimal only at large enough pitch factors: $\alpha_0^2 \geq 2/(\gamma_0 - 1)$. For intermediate values of α_0, viz. $1/\gamma_0 \leq \alpha_0^2 \leq 2/(\gamma_0 - 1)$, the optimal phase velocity corresponds to the interaction with slow waves under the condition of the normal Doppler effect, $\beta_{z,0} < \beta_{ph}$. In the case of even smaller values of α_0 ($\alpha_0^2 < 1/\gamma_0$), the wave phase velocity should be made even smaller, since the optimal is the slow-wave interaction under the anomalous Doppler effect $\beta_{z,0} \geq \beta_{ph}$. Note that under the condition of the anomalous Doppler effect the electrons start their deceleration by losing axial and gaining orbital momentum[61], so in this case it is possible to get coherent radiation even injecting an initially linear electron beam in the interaction space. We will return to the issue of cyclotron resonance masers operation under conditions of normal and anomalous Doppler effects later. Now we will continue discussing the possibilities to identify the optimal conditions for the most efficient operation of relativistic cyclotron masers. One of such conditions was found in [60] and was based on the approach developed in[62]. In that paper, it was shown that the changes in the electron energy in the process of interaction with the plane EM wave can be described by a relatively simple equation for the electron energy

$$\left(\frac{d\gamma}{dt}\right)^2 + V(\gamma) = 0, \tag{4}$$

where $V(\gamma)$ describing an effective potential well is the 4th order polynomial with coefficients depending on a number of parameters characterizing the beam-wave interaction conditions.

The analysis of the polynomial $V(\gamma)$ carried out in[60] resulted in defining the optimal cyclotron resonance mismatch $\delta = 1 - n\beta_{z0} - \Omega_0/\omega$ (here $n = 1/\beta_{ph}$ is the refractive index):

$$\delta_{opt} = \frac{\gamma_0}{\gamma_0 - 1}\beta_{\perp 0} a \cos\varphi_0 + \frac{\gamma_0 - 1}{2\gamma_0}\left(1 - n_{opt}^2\right). \tag{5}$$

In (5), the optimal value of the refractive index is given by Eq. (3), φ_0 is the phase $\varphi = \omega t - k_z z - \theta$ (θ is the gyro-phase) at the entrance. This optimal mismatch depends on three parameters only (γ_0, $\alpha_0 = v_{\perp 0}/v_{z0}$ and $a\cos\varphi_0$, here $a = (\Omega_0/\omega)(E/B_0)$ is the normalized wave amplitude). This optimal mismatch (5), however, depends on the initial phase φ_0, i.e. this condition can be fulfilled for all electrons only in the case of a microbunch of a length much shorter that the wavelength. (Such situation may take place, for example, in class D amplifiers.) An example shown in Fig. 4 reproduced from [60] illustrates the point that, when both conditions ((3) and (5)) hold, an electron with $\gamma_0 = 2$ can be completely decelerated, i.e. at the end of the interaction space $\gamma(z_{end}) = 1$. So, to realize this deceleration it is necessary, first, to form a compact electron bunch and then provide conditions for complete deceleration of electrons in the output waveguide stage of the device.

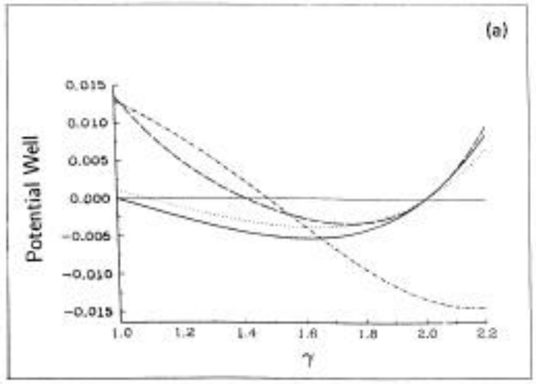

Fig. 4 Potential well in Eq. (4) for different values of the parameters in the polynomial $V(\gamma)$. The solid line shows this well when the conditions given by (3) and (5) hold. In this case, an electron with the initial energy of $511keV$ ($\gamma_0 = 2$) can be decelerated completely ($\gamma(z_{end}) = 1$). In all other cases shown by dotted, dashed and dash-dotted lines, this is impossible.

As follows from the cyclotron resonance condition (1), the wave frequency can be much higher than the electron cyclotron frequency due to the Doppler frequency up-conversion, since Eq. (1) can be rewritten as

$$\omega = \frac{s\Omega}{1 - n\beta_z}. \tag{1a}$$

So, there are, at least, two possibilities to increase the frequency of outgoing radiation operating with given solenoids creating a limited magnetic field: to operate at cyclotron harmonics and/or to operate in the regime of the Doppler frequency up-conversion. A comparative analysis of both sorts of frequency up-shifted devices was carried out in[63]. Figure 5, reproduced from Ref.[63], illustrates these two regimes by two beam lines shown in the $\omega - k_z$ plane.

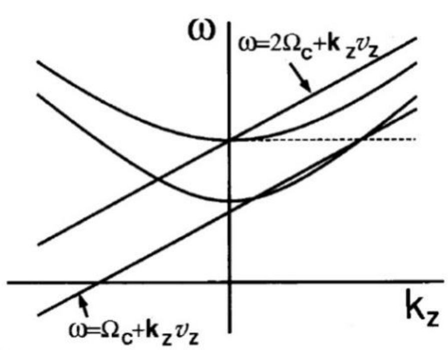

Fig. 5 The waveguide dispersion curves and beam lines for Doppler up-shifted operation at the fundamental and the second harmonic operation near cutoff.

Calculations showed that in the absence of the velocity spread, the Doppler up-shifted regime offers a higher efficiency, but this regime is more sensitive to the velocity spread. So, as the spread increases, sooner or later the harmonic operation near cutoff becomes preferable.

To more accurately analyze the effect of velocity spread on Doppler up-shifted operation, the nonlinear, fully relativistic, multimode, multi-frequency equations were derived by using a Hamiltonian formalism[64]. In these equations, the axial nonuniformity of the waveguides and the tapering of the magnetic field were also incorporated. The equations derived were also used for analyzing the operation stability: first, the start current of parasitic modes in the absence of the desired wave was calculated (zero-drive stability), and then, the suppression of parasitic modes by the operating mode was studied[65].

Effect of magnetic field tapering

The concept of forming an electron bunch and then trapping it for decelerating/accelerating in a properly tapered interaction circuit is widely used in resonance charged particle accelerators as well as in linear-beam traveling-wave tubes and free-electron lasers. An analogous concept of gyro-traveling wave devices was studied in[66]. This concept is illustrated by Fig. 6 reproduced from this paper. The concept is based on fulfillment of the exact cyclotron resonance for a chosen synchronous electron (its phase is denoted by ϑ_s in Fig. 6a) by corresponding tapering of the external magnetic field. This electron remains in the center of the inner ellipse shown in Fig. 6b when the tapering shifts all the curves shown there down. All other electrons with phases different from ϑ_s in the process of beam interaction with the wave of a small amplitude oscillate in the potential well and lose their energy together with the synchronous electron.

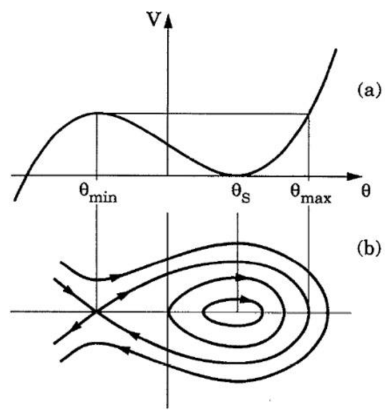

Fig. 6 Potential well (a) and the phase plane (b) for particles interacting with the synchronous EM wave. It is assumed that the magnetic field tapering allows an electron with the phase ϑ_s shown in Fig. 6a to remain in phase with the wave during all interaction process. All other electrons oscillate in the potential well and have energies close to that of the synchronous electron. The electron motion is described by the Hamiltonian given in [66].

Operation with slow waves.

The operation at slow waves can be realized either by using dielectrics (in dielectric-loaded waveguides) or by using slow-wave periodic structures. As discussed in[67], the operation at slow waves, has a number of advantages. First, this operation offers the high efficiency in the case of electron beams with relatively small α_0. As pointed out in[68], such beams are more stable with respect to space charge instabilities in the region of magnetic compression between the MIG gun and the interaction space. Second, as follows from Eq. (1a), the operation at slow waves (their refractive index is $n = 1/\beta_{ph} > 1$) allows one to realize a higher Doppler frequency up-conversion, i.e. to achieve operation at higher frequencies in given magnetic fields. Also, as stated in[68], in the case of slow waves the device can benefit from the absence of intersection of the beam line with the waveguide dispersion curve near cutoff. (As shown in Fig. 5, in the case of fast waves the beam line intersects the dispersion curve twice.) This benefit makes the operation in the Doppler up-shifted regime much more stable. Lastly, the slow-wave CRM amplifiers can operate in a wider frequency band, because the waveguide dispersion curve is not limited by the asymptote $v_{ph} = \omega / k_z = c$. In[68] it was shown that the beam-wave interaction in slow-wave CRMs could be described by slightly modified equations originally derived for fast-wave CRMs. It was shown that profiling of the external magnetic field can diminish the sensitivity of the efficiency to electron velocity spread.

Anomalous Doppler CRMs (AD-CRMs)

In slow-wave CRMs operating under the normal Doppler effect condition the phase velocity is smaller than the speed of light ($n = 1/\beta_{ph} > 1$), but $n\beta_z < 1$. Therefore, as follows from (1a), these devices can operate at any positive harmonic of the electron cyclotron frequency. Radiating electrons in this situation lose both orbital and axial momenta. The anomalous Doppler effect corresponds to the condition $n\beta_z > 1$, hence, as follows from (1a), these devices can operate only at negative cyclotron harmonics. As shown in[61] and discussed in more details in[58, 69, 70], in the case of the anomalous Doppler effect radiating electrons lose axial momentum, but gain the orbital one. Therefore, one can envision an interesting sequence of events in AD-CRMs (no matter whether at the entrance electrons have some initial orbital velocity or move linearly along the external magnetic field): first, electrons will radiate under the condition of the anomalous Doppler effect, i.e. lose their axial momentum and gain the orbital one. Then, when the decreasing axial velocity of a radiating electron reaches the border between the normal and anomalous Doppler effects, i.e. $\beta_z = 1/n$, this electron enters the region of the normal Doppler effect and starts losing both axial and orbital momenta. Correspondingly, when the conditions given by (3) and (5) are fulfilled, such an electron can be completely decelerated. Some attempts to carry out experiments with AD-CRMs were undertaken in the USSR[71, 72], but the reported results were not very convincing.

It was found, however, that in AD-CRMs with constant parameters, the optimal conditions for obtaining the most efficient operation is not easy to realize: the external magnetic field should be very low (so, guiding an intense electron beam can be difficult), the wave electric field should be rather high (so, the RF breakdown becomes a problem) and, finally, the beam-wave interaction should be realized in a very short distance (when electrons make 1-2 orbits only). All this stimulated an interest in studying a concept of AD-CRM with tapered parameters. The results of such a study were presented in Ref.[73]. The nonlinear theory was developed for the AD-CRM operating at the (-1)th cyclotron harmonic and driven by an initially linear electron beam. Optimal taperings of the microwave circuit (e.g., stripline waveguide) and the external magnetic field were found. It was shown that in the limiting case the efficiency could reach 100%, while in a low-power device with a tapered stripline, designed for operating at the 10*GHz* frequency, the calculated efficiency reached the 30% level and the gain was about 25*dB*.

Overlapping of resonances in high-power gyrodevices

The standard description of beam-wave interaction in gyrodevices is based on the assumption that all interaction takes place within the cyclotron resonance at one chosen harmonic of the electron cyclotron frequency. Corresponding changes in electron energies can be understood by seeing the phase space shown in Fig. 6b where all possible trajectories are enclosed in the separatrix limited by the phases $\theta_{\min}$ and $\theta_{\max}$. However, when the wave amplitude is large enough, the changes in the relativistic electron cyclotron frequency caused by the changes in the electron energy in the process of interaction can be on the order of the non-relativistic cyclotron frequency. Then, simultaneous interaction of relativistic electrons with the wave(s) becomes possible at several cyclotron harmonics. Such interaction at three harmonics simultaneously was considered in[74, 75]. In[74], the interaction with a single TE-wave at three cyclotron harmonics ($s = 1, 2, 3$) simultaneously was analyzed. It was assumed that the prime role is played by the second harmonic, but the first and third harmonic interaction can also contribute to the process. Fig. 7 (reproduced from[74]) illustrates the role of this additional harmonic interaction in electron motion: the left figure shows electron trajectories in the case of pure second harmonic interaction; the right figure shows (for the same set of parameters) these trajectories in the presence of the additional interaction at the first and third harmonics. It was shown that this additional interaction results in the destruction of electron periodic motion in the wave of constant amplitude and corresponding Poincare sections reveal all signs of stochasticity in electron trajectories. In Ref.[75] similar processes were studied for the case of simultaneous excitation of three waves (TE_{01}, TE_{02}, and TE_{03}) at the first, second and third harmonics, respectively. The effect of three-wave interaction was analyzed. The cases of the gyro-TWT and gyro-twystron with beam parameters close to the UMD experiments were studied.

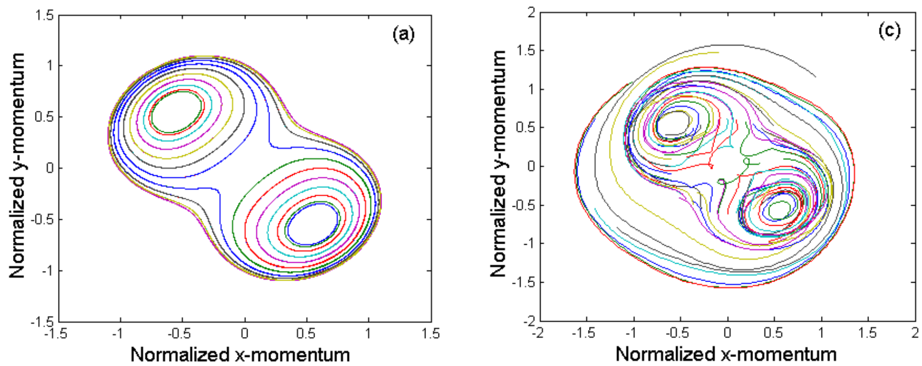

Fig. 7 Electron trajectories in the plane of momentum transverse components in the absence (left) and presence (right) of additional resonances.

Double resonance.

Another special case of simultaneous resonance at two cyclotron harmonics was analyzed in Ref.[76]. This simultaneous resonance is illustrated by Fig. 8 taken from[76].

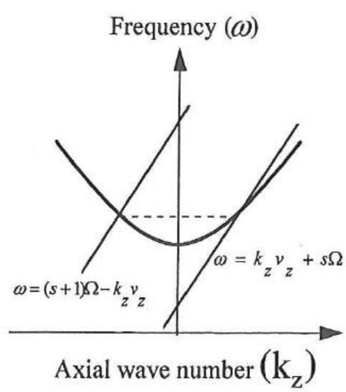

Fig. 8 Simultaneous resonance with the forward wave component of the standing wave at the s-th harmonic and with the backward wave component at the (s+1)-st harmonic.

Here the beam line corresponding to the resonance at the s-th harmonic intersects the waveguide curve at the same frequency of the forward wave component of a standing wave $\sin(l\pi z/L)$, as the beam line corresponding to the resonance at the (s+1)-st harmonic intersects the backward wave component of the same wave. Such double resonance is possible only in resonators of a certain length, when the axial index of the standing wave l, the electron axial velocity and the ratio of the resonator length to the wavelength obeys the condition $L/\lambda = \left[(2s+1)/2\right]\beta_{z0} l$. The Doppler frequency upshift is this regime is equal to $\omega/\Omega = (2s+1)/2$. It was shown in simulations that such double resonance may lead to small increase in the efficiency in the case of symmetric modes, while in the case of rotating modes this resonance always lowers the efficiency.

7. Experimental gyroklystron results

A schematic of our experimental facility is shown in Fig. 8a. Our first two series of tubes were driven by a 1μs flat-top, 500*kV*, 400*A* line-type modulator that had a maximum repetition rate of 4*Hz*. The rise time of the system was about 1.5μs and the fall time was about 1μs. A resistive divider shunted approximately half the current and provided the intermediate voltage required for the double-anode MIG (which was about 70% of the cathode voltage). The original MIG was designed to have an axial velocity spread under 7% at the nominal temperature-limited current of 160*A* (when the average perpendicular to parallel velocity ratio was α=1.5). The nominal cathode loading was about 5.5A/cm^2 and the cathode radius was about 2.3*cm*. The cathode half-angle was 20° and the electron flow was highly non-laminar, resulting in a fairly small range of operating currents that had axial velocity spreads below 10%. For the latter two series of gyroklystrons, we doubled the current capability of our modulator to 800*A* and reduced the maximum rep rate to 2*Hz*. Our new MIG had a single anode, so all the current was available to power the MIG. The velocity spread was designed to be under 6% at 600*A*, and the larger slant angle (from 40° to 42°) allowed for a larger operating range in theory. Two 60-*L/s* ion pumps were connected to a manifold behind the MIG's main anode and two more pumped through a vacuum port in the output waveguide to achieve the required vacuum levels.

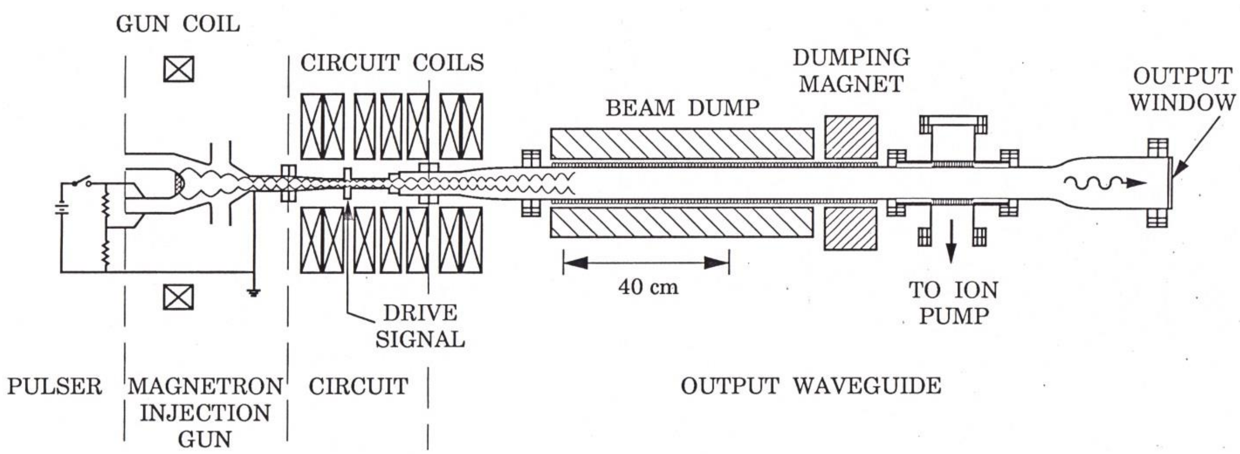

Fig. 8a The experimental test bed for the first two gyroklystron series.

Flexibility in the magnetic field profile was achieved by having four independent power supplies to energize eight water-cooled pancake coils – one near the cathode and seven in the circuit region. The were no magnetic materials in the design, so the code to calculate the magnetic field everywhere with elliptic integrals was quite straightforward. The design magnetic field had a flat region of 25*cm* at 0.565*T* (for the microwave circuit) and a field of 0.047*T* at the cathode center. Experimentally, the magnetic field was routinely tapered in the circuit region to maximize output power. The length of the magnetic compression region was about 48 *cm*. A 2μs, 100*kW*, 9.7-10.0*GHz* (mechanically tunable) coaxial magnetron provided the input power, which was injected radially into the first cavity. A high-power variable attenuator was used to adjust the drive power in most of the experiments. A calibrated set of X-band directional couplers, attenuators, and crystal detectors were used to monitor the incident and reflected drive power. The amplified power was extracted axially and traveled through a nonlinear tapered wall section, the beam dump, and a second tapered region to a 12.7*cm* diameter BeO half-wavelength output window. An anechoic chamber was used for preliminary stability and amplification studies and a directional coupler/liquid calorimeter system was used for high-power amplification measurements.

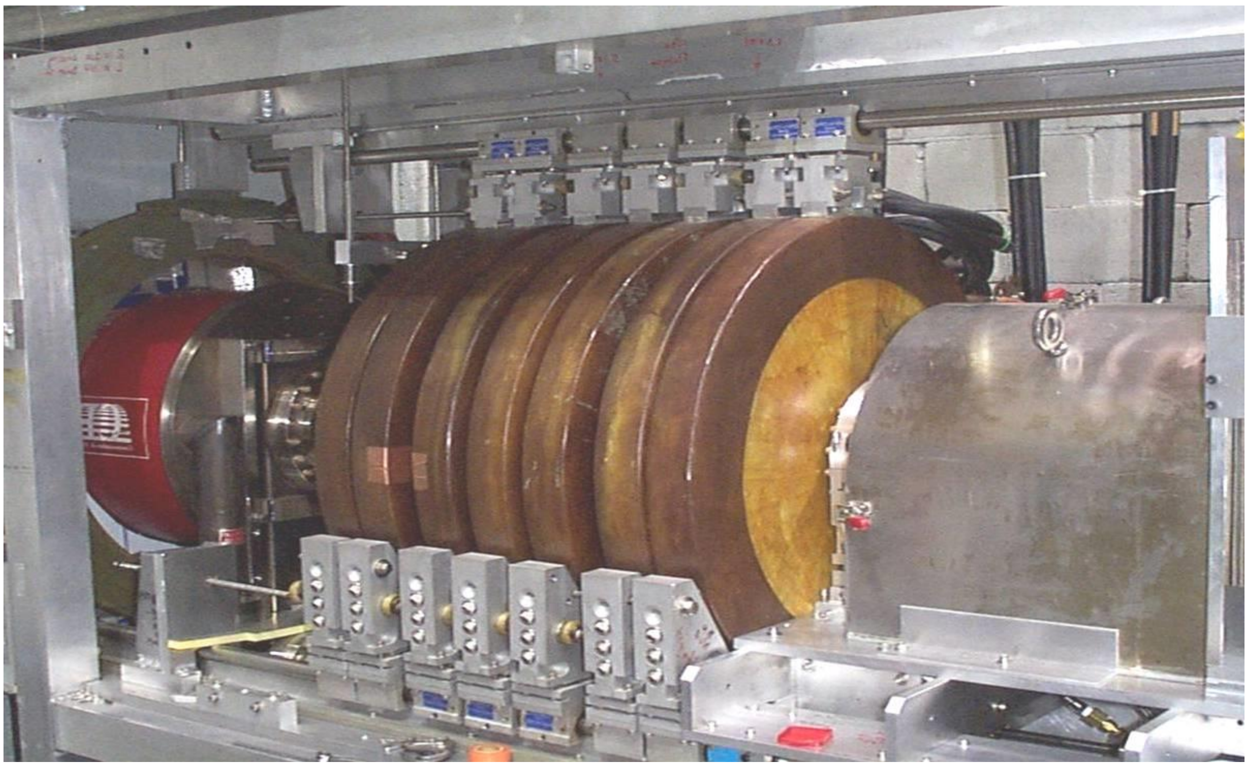

Fig. 8b The UMD experimental test bed.

A side view of the experimental test bed is shown in Fg. 8b. The output waveguide can not be seen due to the surrounding hardware. The Magnetron injection gun is housed in the red can at the left of the picture. The seven main-field pancake coils (on moveable rails) are in the center of the photo and the lead shield surrounding the beam dump is on the right of the photo. Fig. 8c shows a view down the end of the test bed. The output window is removed, so the inside contours of our nonlinear tapers can be seen. The dump magnet coil sits at the top of the photo.Without it, enough current would hit the half-wavelength alumina window (shown in Fig. 8d) to destroy the vacuum seal. Flanges where vacuum ion pumps are normally connected are covered with foil and sit to the left and the right of the output waveguide.

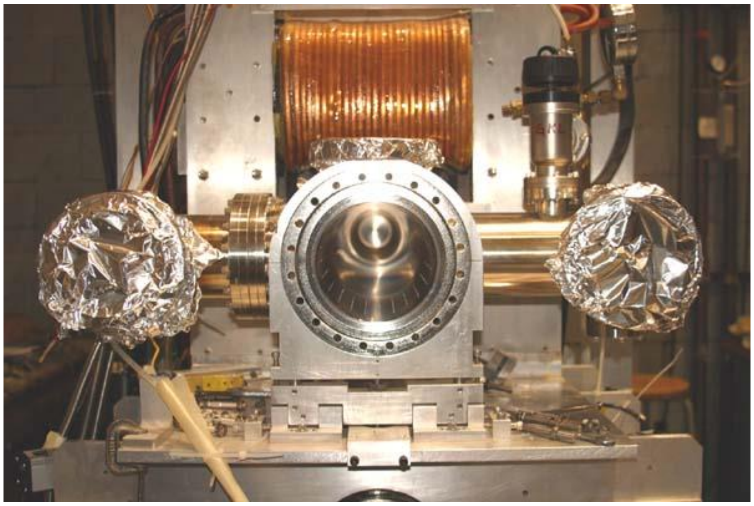

Fig. 8c The end view of the output waveguide and surrounding hardware.

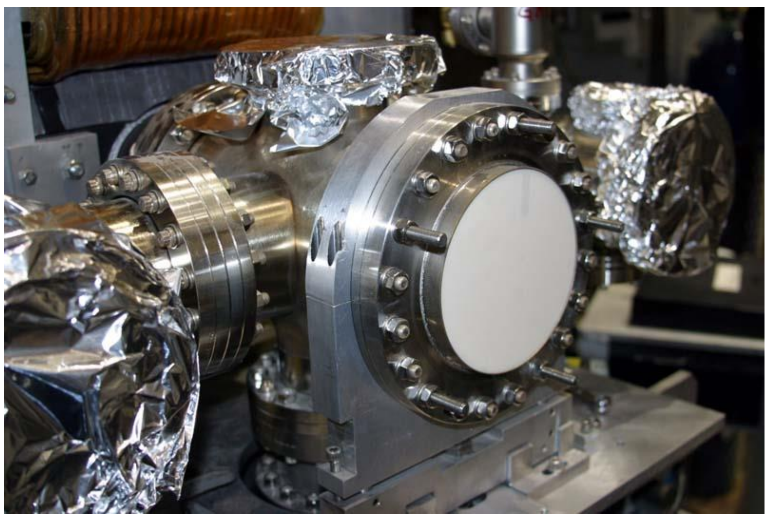

Fig. 8d An oblique view of the output waveguide with the ouptput window attached.

The quality factor (Q) in all input cavities was adjusted for critical coupling by using a thin lossy-ceramic ring placed against a sidewall. The buncher cavity Qs (in tubes that had them) were derived predominantly from lossy ceramics on a sidewall, but could also be impacted by adjacent ceramics in the drift tube. The output cavity Q was predominantly due to diffractive losses from the cavity's output lip. The Q factors in all cavities spanned the range from 50 to 575 in the various tubes.

Table IV summarizes all of the key amplification results for the entirety of the GKL experimental program. For the first series (fundamental circular tubes), a total of six two-cavity and four three-cavity gyroklystron tubes were tested. The search for the optimal operating point involved the systematic variation of beam voltage and current, drive frequency, magnetic field profile, and beam velocity ratio (via magnetic compression). The first two tubes were plagued by a multitude of instabilities, produced power levels below 50*kW*, and had signal gains somewhat less than 0*dB*. Instabilities could be divided in four groups. Modes in the first group existed mainly in the output waveguide in frequency ranges where the window was a good reflector. These modes were suppressed by amplifier operation. The second group existed in the output waveguide adjacent to the output cavity and required significant reflections from the first nonlinear taper. "Whole tube" modes comprised the third group and had their energy mainly in the drift tube with reflections provided by the cavities. The final mode class included instabilities in the MIG downtaper. Instabilities in the latter two groups were the most difficult to suppress and ultimately limited tube performance.

Tab. IV Summary of the best experimental, measured results for the UMD GKL program. All tubes are gyroklystrons, unless the tube type indicates a (right circular) gyro-twystron.

Output harmonic #	# of cavities	Tube Type	Output Frequency (*GHz*)	Peak Power (*MW*)	Peak efficiency (%)	Saturated gain (*dB*)
1	2	Circular	9.87	24	31	26
1	3	Circular	9.86	27	32	36
2	2	Circular	19.76	32	29	27
3	2	Circular	29.63	1	1	12
1	1	Twystron	9.88	22	21	24
2	1	Twystron	19.76	12	11	21
1	3	Coaxial	8.60	80	30	30
2	3/4	Coaxial	17.14	27	10	26

Tube 3 had markedly improved attenuation in the downtaper region and drift tube, allowing significant beam power to be injected into the circuit and resulted in a one and a half order of magnitude increase in the output power. Tubes 4 and beyond had a linear wall taper after the output cavity lip. Tube 4 produced peak powers near 2.7*MW* in a constant magnetic field. Tube 5 incorporated even more loss in the downtaper and had a higher output cavity Q (225). The primary performance increase, however, came from a negative tapering of the magnetic field by about 15% over the tube length. The maximum power was 24*MW*, the maximum efficiency was 31%, and the gain exceeded 26*dB*. The nominal beam parameters were simulated with MAGYKL and theoretical efficiency was in good agreement with the measured result. The output cavity Q in Tube 6 was increased to about 500, for which 160*A* was 80% of the start current for the TE_{011} mode. We found two good operating points with this tube. The first was the maximum efficiency point, where 22*MW* was produced near 9.87*GHz* with an efficiency of 34% and a gain of 34*dB*.

The second operating point had a maximum power level of 24*MW*, but with 26% more current, hence lower efficiency.

The photo in Fig. 9 shows the vacuum housing (at the top of the photo) and all of the key components for our final fundamental-mode, two cavity, circular gyrolystron. The input cavity components are on the left side of the photo, including the input window, the stainless-steel ring that defines the cavity dimensions, two copper endwalls and the carbon-impregnated aluminosilicate (CIAS) ceramics that provide critical coupling for the cavity. The three metal rings on the far right of the figure comprise the TE_{011} output cavity. The eleven rings in the middle make up the drift region (eight gray BeO ceramics and three metal rings).

Fig. 9 The actual unassembled hardware for Tube 6.

The fundamental mode three-cavity tubes had a tunable buncher cavity. Tuning was achieved with two metal rods whose insertion distance could be controlled remotely and could adjust the resonant frequency by up to 90*MHz*. The rods had rounded ends and no breakdown problems were ever observed. These tubes also used exclusively our “home-made” aluminosilicate lossy ceramics in the drift tubes. In all but the first three-cavity device, the downtaper also used only our homemade lossy ceramics. The best power performance of the two- and three-cavity tubes was similar at the 15% tapered field profile. The gain of the three-cavity tubes was typically improved over that of the two-cavity tubes, with a maximum saturated gain of 50*dB* occurring at an operating point that produced 21*MW*. A maximum peak power of 27*MW* was obtained with an efficiency of 32% with a 30% taper in magnetic field in tube 8.

For our second series of gyroklystrons, seven second-harmonic tubes were designed, fabricated and tested. The first tube was derived from the two-cavity first harmonic system by making minor modifications to the drift tube and by replacing the fundamental output cavity with one that resonated at twice the drive frequency in the TE_{021} mode. The input cavity quality factors ranged from 225 to 500 in all tubes. The first three second-harmonic tubes had resonant traps in the drift tube to isolate the input cavity from any TE_{01} signal at 19.7*GHz* that might come back from the output cavity. The resonant trap for the first tube was fabricated with two lossy ceramic rings, comprised of SiC (1%) and MgO (99%), that were tuned to the needed resonant frequency by adding small air cavities to the oxygen free high conductivity (OFHC) copper rings adjacent to the ceramic rings. The traps for Tubes 2 and 3 were designed with the aid of the scattering matrix code. They both utilized thin slightly lossy dielectric cavities made from CIAS rings and an axially thin cavity designed to resonate in the TE_{021} mode at twice the drive frequency. In Tube 3, the resonant cavity was actually loaded with a slightly lossy CIAS ring to increase the bandwidth of the filter in K-band. Tube 3's maximum attenuation in X-band was near 40*dB* around 10.5*GHz* and was above 45*dB* at 19.72*GHz* in K-band. The resonant traps were found during amplification studies to be unnecessary and to have a deleterious effect on tube stability at lower frequencies, so they were replaced in Tubes 4 and beyond with four additional tapered BeO-SiC rings. This change decreased the attenuation in K-band to a nearly constant 10*dB*. The fifth tube had a capacitive probe inserted nearly midway into the drift region. Tubes 6 and 7 started with the geometry of the fourth tube and added an inner conductor that was supported by tungsten pins in the drift tube. The diameter of the assembly was 0.4*cm* and it extended from the preliminary drift space through the input cavity and drift space and terminated at the entrance to the output cavity.

The output cavities were designed with maximum radii that precluded amplification at the drive frequency in the TE_{011} mode. All but one of the harmonic tubes (#5) had smoothly varying wall transitions to minimize mode conversion. Tubes 1 through 3 had different output cavities, with the length of the main section becoming progressively shorter. The scattering matrix code predicted the TE_{02} mode to be 99.4% pure and the power flowing into the drift tube to be down from the output power by over 38*dB*. This output cavity was also used for the fourth, sixth, and seventh tubes. The fifth tube had a stepped output cavity with a mixed TE_{01}/TE_{02} mode, for which the mode purity varied widely with beam parameter adjustments. The step was designed to minimize power flow into the drift region, which was at least 24*dB* below the output power level. The overall length of this cavity was 82% less than the third smooth-walled cavity.

As with the fundamental tubes, the main parameter variations of interest included beam voltage, beam current, velocity ratio α, input cavity magnetic field, output cavity magnetic field, and drive frequency. The optimal drive power for the later tubes was typically near 60*kW*. As instabilities were systematically eliminated from Tubes 1 through 4, the output power steadily increased. The long relatively flat output cavity of the first tube exhibited numerous oscillations. The second tube exhibited a significantly enlarged region of stability. This tube ultimately produced 12*MW* at 19.742*GHz*. Tube 3 showed significant improvement with respect to background instabilities because of a shorter output cavity. A maximum output power of over 21*MW* at 19.757*GHz* was achieved with an efficiency of 21% and a gain of 25*dB*. Tube 4 produced a peak power point of approximately 32*MW* with a beam current of 244*A*, a flat top beam voltage of 457*kV*, and a drive frequency of 9.882*GHz*. The variation of voltage across the pulse resulted in the triangular-looking rise and the narrowing of the output pulse width. The efficiency of the high power point was almost 29% and the large signal gain was over 27*dB*. From far-field radiation patterns, the mode purity in the TE_{02} mode was estimated to be over 99%.

The fifth tube utilized a short mixed-mode output cavity and exhibited a stable operating range that was considerably larger than its longer smooth-walled counterparts [77]. Unfortunately, the maximum peak amplified power was only about 20*MW* at 19.78*GHz*, with an efficiency of 23% and a gain of 26*dB*. The mode mixture near the optimal operating point was 60% TE_{02} and 40% TE_{01}; this was close to the cold cavity simulated results. In Tube 5, the capacitive probe was used to measure the beam's charge density, and in conjunction with voltage and current measurements, infer the average velocity ratio[78]. These measurements were performed over a wide range of voltages, currents, and magnetic compressions. At parameters near the optimal peak power points (e.g., beam voltages and currents in excess of 400*kV* and 200*A*, respectively, and magnetic compressions near 12), the measured average velocity ratios were consistently above the velocity ratios computed by EGUN by 30-40%. This discrepancy represented a significant increase in perpendicular energy and could easily explain why a number of first- and second-harmonic tubes outperformed the theoretical efficiencies by several percent. It was estimated that this discrepancy could be explained in part by the reduction in cathode magnetic field due to the beam's rotational motion (an effect that was not calculated by EGUN).

Tubes 6 and 7 had thin coaxial inserts that were developed in part to test some of the concepts related to later experiments (described later in this section)[79]. In general, they were more stable than their right-circular predecessors and had maximum stable compressions approaching a factor of 13. However, beam clearance was predicted by simulations to be tight, and current scrape-off limited the accessible range of magnetic fields. As a consequence, we could not get back to the optimal operating point of Tube 4. The maximum repeatable peak powers produced in Tubes 6 and 7 were 13 and 21*MW*, respectively. The coaxial tube experiments were cut short by different failure mechanisms of the inner conductor support structure. Lessons learned from these two tubes were used to improve the third and fourth gyroklystron tubes sequences, which had substantial inner conductors.

A single third-harmonic tube was investigated by replacing the output cavity of the fourth second-harmonic tube with one that resonated in the TE_{031} mode at three times the fundamental drive signal[80]. This cavity had slowly varying radial wall transitions to minimize mode conversion and had a radius in the main section that prevented second-harmonic operation in the TE_{021} mode. The large-signal code predicted a maximum efficiency of about 11% with a fairly strong magnetic field uptaper and an output cavity quality factor of about 700. The third-harmonic output cavity realized resonant frequency was 29.57*GHz* and a Q of only 525 due to manufacturing issues. The tube produced only about 1*MW* of peak power - considerably less power than expected and was extremely sensitive to beam parameters and instabilities (predominantly a TE_{11} mode near 7.1*GHz*). No additional third-harmonic systems were attempted due to poor theoretical efficiency predictions and worse experimental results.

In Fig. 10, the shapes of the output cavities from each of the maximum power-producing two-cavity tubes are contrasted. Note that the y-axis has been offset and considerably expanded. The first-harmonic tube (dashed line) had sharp wall transitions and a short disk-like coupling lip. The dimensions were determined by resonance, stability, and efficiency calculations. The only restriction on the maximum radius came from requirement that the TE_{02} mode be cut off at 9.87*GHz* everywhere in the cavity, and the nearby output waveguide and was not a factor in the design. Both the second- (solid line) and third-harmonic (dot-dashed line) cavities had smooth radial wall transitions to minimize mode conversion. The restriction that the wall radius be small enough to be cut off to lower radial modes at lower harmonics and yet be large enough so that the desired radial mode was above cutoff became increasingly difficult to satisfy with increasing harmonic number. To complicate matters, the required quality factor for optimal efficiency also generally increased with harmonic number.

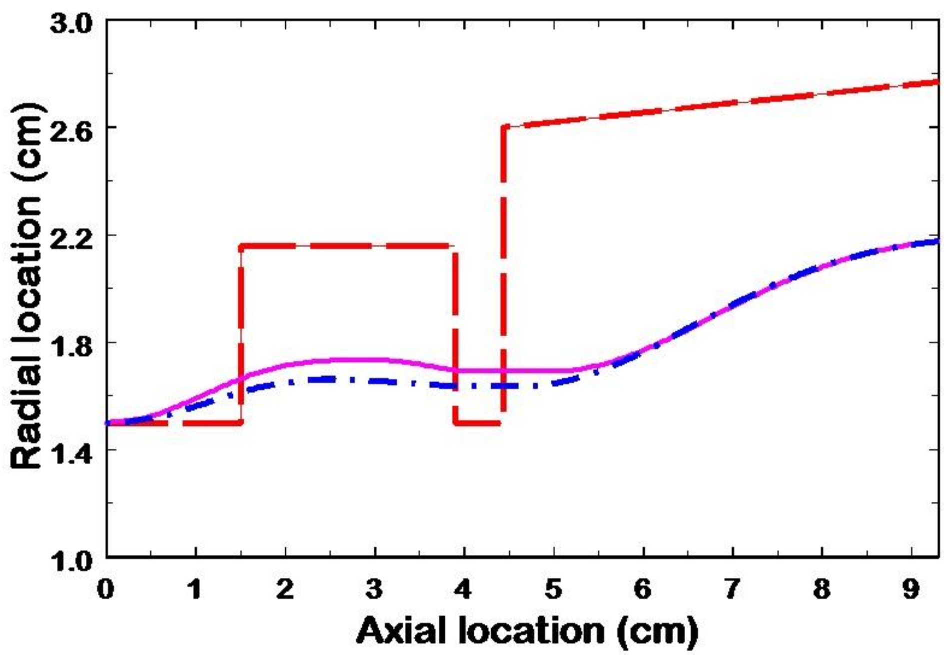

Fig. 10 A comparison of the output cavities for the first, second, and third harmonic right-circular gyroklystron tubes.

In our quest to produce over 100*MW* with a gyroklystron, we chose to increase the beam power predominantly by increasing the beam current. While higher modulator voltages are possible with current pulse forming network (PFN) technology, we wanted to remain in line with the current SLAC klystron designs. Furthermore, we chose to keep the beam density in the new system about the same as in the previous experiments in order to keep the demands on the cathode loading and the magnetic compression modest. This approach is consistent with high-quality beam production and long-lifetime devices. The choice of beam density necessitated a three-fold increase in beam radius to about 2.4*cm*, which meant that either a new operating mode had to be selected or that the drift tube was no longer be cut off to the operating mode. We decided to go with a new mode that was similar to the old one, namely to use the circular electric modes, but to introduce an inner conductor to maintain intercavity isolation[40]. This conductor would ultimately be supported in a production tube (mounted vertically) in the beam dump. However, because our test bed was horizontal, we used tungsten pins in the drift regions to support the conductor. Finally, we chose to decrease our drive frequency to a multiple of the SLAC frequency (8.568*GHz*). The concomitant reduction in required magnetic field added some flexibility to our magnetic field configuration.

Our three-cavity, coaxial, fundamental mode gyroklystron circuit is shown in Fig. 11. The inner conductor extends well into the downtaper region and ends with a linear taper soon after the output cavity lip. It is supported by 2*mm* diameter tungsten pins in the drift regions just before the input and output cavities. The pins were expected to intercept no more than 3% of the beam and survive a 1*Hz* repetition rate. The pins did experience more erosion than expected but did not cause issues with the vacuum levels in the tube. In the drift regions, a single layer of lossy ceramics lined the inner conductor and a double layer of lossy ceramics lined the outer wall. All cavities operated in the TE_{011} mode; the input and buncher cavities were defined exclusively by indentations on the inner conductor while the output cavity had transitions on both the inner and outer walls to place the beam in the maximum electric field of the operating mode.

While the tube was expected to produce over 100*MW* of peak power with over 40% efficiency when the velocity ratio of 1.5, instabilities forced operation at parameters for which the velocity ratio was estimated to be about 1.05. The maximum efficiency of 31.5% required a beam voltage of 470*kV* and a peak current of about 500*A*. The tube was driven at 8.6*GHz* and had a large-signal gain of nearly 30*dB*. The microwave pulse had a 3*dB* width of 1.7μs and a peak power of 75*MW*. Peak powers in excess of 80*MW* were achieved at slightly lower efficiencies. These experimental results agreed extremely well with theoretical calculations with the modified beam parameters [27, 28].

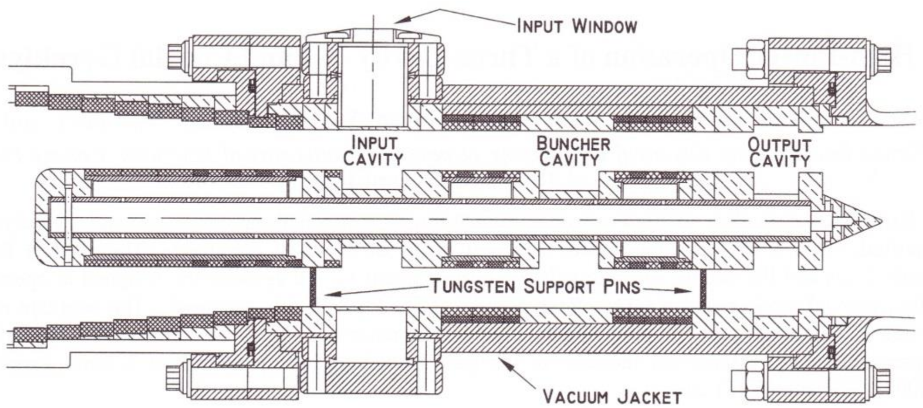

Fig. 11 The three-cavity, first harmonic, coaxial gyroklystron circuit. Taken from [27].

The final tube series of the University of Maryland Gyroklystron Program had as a goal the production of 80*MW* of peak power at 17*GHz*, using a 500*W*, 500*A* electron beam interacting with three and four cavity second-harmonic coaxial gyroklystrons. The input cavity was taken from the fundamental mode coaxial tube and operated in the TE_{011} mode near 8.568*GHz*. The second harmonic buncher and output cavities were defined by symmetric indentations on the inner and outer conductors and operated in the TE_{021} mode near 17.136*GHz*. The quality factor of the output cavity came predominantly from the diffractive lip. The quality factor of the buncher cavity was derived primarily from adjacent lossy ceramics in the drift tube[81].

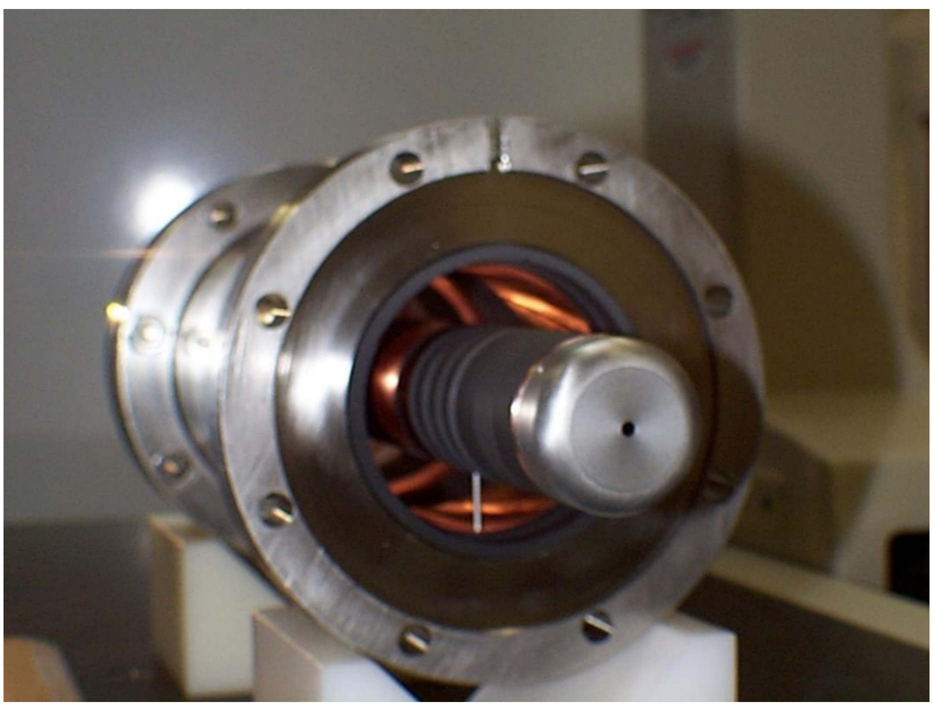

Fig. 12 The second harmonic coaxial gyroklystron circuit.

A photo of the second-harmonic coaxial gyroklystron circuit before insertion into the test bed is shown in Fig. 12. The photo is looking down the tube, so the inner conductor seen was inserted into the downtaper of the magnetron injection gun. The photo clearly shows the lossy ceramics on the insert as well as one of the two thin tungsten pins that supported the inner conductor. The coaxial insert for a three-cavity second-harmonic tube is shown in Fig. 13. Lossy ceramics before the input cavity have been assembled, but the lossy ceramics on either side of the second-harmonic buncher cavity are missing (they go over the stainless steel sections. The input cavity is defined by the deep indentation to the right of the main ceramic stack. (Recall that the cavities are also defined by wall-radii changes on the outer conductor.) The right-most ceramic in the photo is inside the input cavity and helps to define the Q. The other two copper indentations define the second-harmonic cavities. The long linear downtaper terminates the inner conductor and is at the same axial location as the nonlinear taper on the outer conductor.

Fig. 13 The coaxial insert for the second-harmonic coaxial gyroklystron circuit.

The second-harmonic coaxial tubes never produced peak powers above 27MW[105]. The root cause of the inability to achieve the desired peak power performance was the non-uniform emission from the temperature-limited magnetron injection gun (MIG). The azimuthal current density varied by more than +/- 50% due in large part to a 60°C temperature variation on the emitter surface. The faulty MIG was replaced with a second single-anode MIG that was designed to have superior azimuthal current uniformity, but that MIG suffered from insurmountable vacuum problems and the experimental component of the GKL program came to an end.

8. Gyro-twystron studies

Both theoretical development (discussed previously) and experimental investigations of gyro-twystron microwave tubes occurred during the course of the GKL project [51, 52]. Whereas the gyroklystron used exclusively microwave cavities separated by drift regions, the final stage of the gyro-twystron was a traveling-wave section. Hence, gyro-twystrons should inherently have had better bandwidth properties than gyroklystron devices, unless bandwidth was determined predominantly by the input or buncher cavities.

Two gyro-twystron tubes were tested. The first tube was designed to operate near 10*GHz* at the fundamental gyrotron frequency and the second tube was designed to operate near 20*GHz* at the second harmonic. Both tubes were based on the low-power TE_{011} circular gyroklystron tubes. Both gyro-twystrons utilized the downtaper and input cavity of the gyroklystron devices. Both drift regions were similar to the gyroklystron drift tubes, though the second harmonic device had some modifications to the center of the drift region to enhance high frequency losses. Both devices had fairly long output waveguides, though the second harmonic tube had a smaller radius to cut off the TE_{01} mode at the operating frequency.

During testing, a maximum average perpendicular-to-parallel velocity ratio approximately equal to one was used to avoid oscillations. The axial magnetic field profile was heavily (negatively) tapered in the output section to maximize efficiency. Peak powers above 21*MW* were achieved in 1μs pulses with an efficiency exceeding 22% and a large signal gain near 24*dB* in the first harmonic tube. The second harmonic tube achieved nearly 12*MW* of the peak power with an efficiency of 11% and a gain above 21*dB*. First harmonic amplifier performance was limited principally by competition from a fundamental mode output waveguide interaction while the second harmonic tube was limited by both travelling wave output modes and by a downtaper oscillation. While tube modifications may well have enhanced peak power performance for both gyro-twystron tubes, no significant advantages were uncovered for the accelerator application, so the gyro-twystron experiments were discontinued in favor of additional gyroklystron experiments.

9. Depressed collector studies

Two different theoretical studies were performed to see if depressed collectors could be used with the gyroklystron to enhance efficiency and decrease overall wall plug power and cooling issues. If possible, this would allow gyroklystrons to appear more favorably compared to klystrons, which often have efficiencies in excess of 50%. The first device featured a three-stage depressed collector of conventional design[84]. This device would require radial extraction of the microwave power, as compared to the axial extraction actually used in the gyroklystron experiments[83]. Computer simulations with a standard model for secondary emission and a model of electron distribution from our MAGYKL code indicated that the collection efficiencies as high as 76% were attainable. With gyroklystron peak efficiencies typically as high as 30%, the overall device efficiency could be as high as 64%. This design would have had significant additional capital costs, due to added complexity of the power source and microwave tube, which would have presumably been more than offset by the reduced operating costs.

The second design involved only a single-stage depressed collector[85]. The simplicity of its design was its main advantage, for example, the axial microwave power extraction was still viable. However, simulations showed that this design only enjoyed a modest enhancement in efficiency. For example, a gyroklystron efficiency of 30%, coupled with a collector efficiency of about 53%, lead to a net efficiency of less than 48%. Neither design was realized during the course of the GKL project.

10. Impact of the UMD GKL project

The GKL project at the University of Maryland has had, and continues to have years later, a measureable impact on other projects around the globe. Of particular utility are the codes developed for gyroklystron analysis (the scattering matrix codes, the small signal QPB and the large-signal MAGYKL), the analysis and application of lossy dielectrics as microwave absorbers, and the design procedures used to realize all subsystems of gyro-amplifiers. A few of the programs that have benefited from our work are mentioned below.

A collaboration of industry (CPI), government (NRL), and university (UMD) personnel developed, built and tested a W-band gyroklystron to be the source for the WARLOC radar system [86-92]. This collaborative group was actually awarded the R.L. Woods Award for Excellence in Microwave Sources in 1999. The development relied heavily on the work at UMD, including code use and the drift tube design methodology with lossy dielectrics. The WARLOC tube produced 10*kW* average power (92*kW* peak power) near 94*GHz*[88].

Other work at the Naval Research Laboratory benefitted from the GKL program, including general theoretical design of gyroklystrons,[93, 94], 35*GHz* gyroklystrons[95-97], Ka-band gyro-TWTs [98-101], and general gyro-amplifier stability[102]. The theoretical studies utilized all our codes and design techniques, the experimental Ka-band tubes also generally benefitted from our drift-tube stability work. The general gyro-amplifier paper investigated higher-order mode excitations in the up-taper region beyond the output cavity, and utilized the experience gained from studies at UMD of post-cavity excitations, instabilities, mode conversion, and radiation pattern analysis. It particularly benefited from the UMD work involving the use of a deliberate mixed-mode output cavity[77].

The impact of the GKL program extends well beyond the Naval Research Laboratory. For example, a recent paper from researchers in India is a direct follow-up analysis to the UMD high power gyro-twystron work, and uses that work as the subject of further simulations and as data for model validation[103]. Another recent paper from researchers in Russia cites the UMD gyroklystron work[104].

11. Conclusions

The gyroklystron project measurably advanced the state-of-the-art, not just for pulsed gyroklystron devices, but also for a number of subsystems needed for beam production, tube stabilization, and microwave mode conversion, as well as advancements in theoretical modeling of cold cavity characteristics and small-signal analysis and the large signal behavior of gyro-devices. Peak power results of about 80*MW* of peak power with a fundamental-mode coaxial gyroklystron near 8.6*GHz* and 30*MW* in a second-harmonic gyroklystron operating near 19.76*GHz* represented advances of several orders of magnitude in peak power of previous gyroklystrons. The later result also represented the state of the art in peak power density for microsecond amplifiers at the time. While the project began to wind down a decade ago, products of the research effort research have had, and continue to have, a significant impact on the gyro-amplifier development community.

Acknowledgements

There were far too many students, staff and faculty involved with this project to name them all here; what follows is a partial list of the key contributors to the effort with apologies to those whose names are omitted. First, we would like to thank DOE-HEP and personally Dr. D. Sutter for the support throughout the length of this project. Clearly, we are also indebted to those who launched the project: Profs. V. Granatstein, the late M. Reiser, and C. D. Striffler. We would also express our appreciation for the efforts of K. R. Chu, P. E. Latham, the late J. M. Baird, H. W. Matthews, J. Cheng, M. Castle, S. Tantawi, S. Tiwari, P. Purohit, K. Bharathan, H. Raghunathan, G. P. Saraph, W. Main, A. Singh, M. E. Read, L. Ives, J. Neilson, W. X. Wang, M. Caplan, M. K. E. Flaherty, V. Irwin, M. Arjona, M. Skopec, D. Reichenthal, and M. L. Naiman.

References

[1] W. M. Bollen, A. H. McCurdy, B. Arfin, et al. “Design and Performnance of a Three-Cavity Gyroklystron Amplifier”.*IEEE Trans. Plasma Sci*., 13, 417-423 (1985).

[2] A. H. McCurdy, C. M. Armstrong, W. M. Bollen, et al. "Improved Oscillator Phase Locking by Use of a Modulated Electron Beam in a Gyrotron".*Phys. Rev. Lett*. 57, 2379 (1986).

[3] K. R. Chu, L. R. Barnett, W. K. Lau, et al. "A wide-band millimeter-wave gyrotron traveling-wave amplifier experiment".*IEEE Trans. Electron Devices*, 37, 1557-1560 (1990).

[4] R. S. Symons and H. R. Jory. "Cyclotron Resonance Devices".*Advances in Electronics and Electron Physics*, edited by C. Martin (New York: Academic Press),55, 1-75 (1981).

[5] T. G. Lee, G. T. Konrad, Y. Okazaki, et al. "The Design and Performance of a 150-MW Klystron at S Band".*IEEE Trans. Plasma Sci*., 13, pp. 545-552 (1985).

[6] V. L. Granatstein, K. R. Chu, A. Drobot, et al. "Design of Gyrotron Amplifiers for Driving 1 TeV$e^{+}-e^{-}$ Linear Colliders".*IEEE Trans. Nucl. Sci.*NS-32,2957(1985).

[7] K. R. Chu, V. L. Granatstein, P. E. Latham, et al. "A 30 MW Gyroklystron Amplifier Design for High Energy Linear Accelerators".*IEEE Trans. Plasma Sci.*PS-13, 424-434 (1985).

[8] V. L. Granatstein and W. Lawson. "Gyro-Amplifiers as RF Drivers for Multi-TeV Linear Colliders".*IEEE Trans. Plasma Sci.*24, No. 3, 648-664 (1996).

[9] K. L. Felch, B. G. Danly, H. R. Jory, et al. "Characteristics and Applications of Fast-Wave Gyrodevices".*Proc. IEEE*, 87, 5, 752-781 (1999).

[10] J. M. Baird and W. Lawson. "Magnetron Injection Gun (MIG) Design for Gyrotron Applications".*Int. J. Electronics*,61, 953-967 (1986).

[11] W. B. Herrmannsfeldt. "Electron Trajectory Program". *SLAC Rep.* 226(1979).

[12] M.Caplan and C. Thorington. "Improved Computer Modeling of Magnetron Injection Guns for Gyrotrons".*Int. J Electron*.,51, 415-426 (1981).

[13] W. Lawson, J. Calame, V. L. Granatstein, et al. "The Design of a High Peak Power Relativistic Magnetron Injection Gun".*Int. J. Electronics*,61, 969-984 (1986).

[14] R. T. Longo, IEDM Tech. Digest, 467(1981).

[15] W. Lawson and V. Specht. "Design Comparison of Single-Anode and Double-Anode 300 MW Magnetron Injection Guns".*IEEE Trans. Electron Dev*.,40, 1322-1328 (1993).

[16] W. Lawson. "Magnetron Injection Gun Scaling". *IEEE Trans. Plasma Sci*.,16, 290 (1988).

[17] W. Lawson, H. Raghunathan, and M. Esteban. "Space-Charge Limited Magnetron Injection Guns for High-Power Gyrotrons".*IEEE Trans. Plasma Sci*.,32, 1236-1241 (2004).

[18] H. Raghunathan and W. Lawson. "The Design of Space-Charge Limited Magnetron Injection Guns with Control Electrodes for Gyroklystron Applications".*IEEE Trans. Plasma Sci*., 33, 1366-1371 (2005).

[19] M. E. Read, G. Nusinovich, and R. L. Ives. "Design of An Inverted Magnetron Gun for a High Power Gyroklystron".*High Energy Density and High Power RF: 6th Workshop*, edited by S. H. Gold and G. S. Nusinovich (American Institute of Physics), 136 (2003).

[20] J. Calame and W. Lawson. "A Modified Method for Producing Carbon Loaded Vacuum Compatible Microwave Absorbers from a Porous Ceramic".*IEEE Trans. Electron Dev*. Part 2.38, 1538-1543 (1991).

[21] J. Calame, W. Lawson, V. L. Granatstein, et al. "Experimental Studies of Stability and Amplification in Four Overmoded, Two-Cavity Gyroklystrons Operating at 9.87 *GHz*".*J. Appl. Phys*.,70, 2423-2434 (1991).

[22] W. Lawson, J. Calame, B. Hogan, et al. "Efficient Operation of a High Power X-Band Gyroklystron".*Phys. Rev. Lett*.,67, 520-523 (1991).

[23] W. Lawson, J. Calame, B. Hogan, et al. "Performance Characteristics of a High Power, X-Band, Two-Cavity Gyroklystron".*IEEE Trans. Plasma Sci*.,20, 216-223 (1992).

[24] S. Tantawi, W. Main, P. E. Latham, et al. "High Power X-Band Amplification from an Overmoded Three-Cavity Gyroklystron with a Tunable Penultimate Cavity".*IEEE Trans. Plasma Sci*.,20, 205-215 (1992).

[25] W. Lawson, H. W. Matthews, M. K. E. Lee, et al. “High Power Operation of a K-Band Second Harmonic Gyroklystron”.*Phys. Rev. Lett.*,71, 456-459 (1993).

[26] H. W. Matthews, W. Lawson, J. P. Calame, et al. “Experimental Studies of Stability and Amplification in a Two-Cavity Second Harmonic Gyroklystron”.*IEEE Trans. Plasma Sci*.,22, 825-833 (1994).

[27] W. Lawson, J. Cheng, M. Castle, et al. "High Power Operation of a Three-Cavity X-Band Coaxial Gyroklystron".*Phys. Rev. Lett*., 81, 3030-3033 (1998).

[28] J. Cheng, X. Xu, W. Lawson, et al. “Experimental Studies of a High-Power, X-Band, Coaxial Gyroklystron”.*IEEE Trans. Plasma Sci.*, 27,1175-1187 (1999).

[29] W. Wang, W. Lawson, and V. L. Granatstein. “The Design of a Mode Selective Directional Coupler for a High Power Gyroklystron”.*Int. J. Electronics*,65, 705-716 (1988).

[30] W. Lawson, M. E. Read, W. Wang, et al. “An Evaluation of Directional Couplers for High Power Gyrotrons”.*Int. J. Electronics*,72, 1135-1144 (1992).

[31] W. Lawson. “Theoretical Evaluation of Non-Linear Tapers for a High Power Gyrotron”.*IEEE Trans. Microwave Theory Tech*.,38, 1617-1622 (1990).

[32] J. Neilson, P. E. Latham, M. Caplan, et al. “Determination of the Resonant Frequency in a Complex Cavity using the Scattering Matrix Formulation”.*IEEE Trans. Microwave Theory Tech*.,37, 1165-1170 (1989).

[33] W. Lawson. “Theoretical Mode Conversion in Overmoded Non-linear Coaxial Waveguide Tapers”.*IEEE Trans. Microwave Theory Tech*.42, 127-131 (1994).

[34] W. Lawson and P. E. Latham. “The Scattering Matrix Formulation for Overmoded Coaxial Cavities”.*IEEE Trans. Microwave Theory Tech*.,40, 1973-1977 (1992).

[35] W. Lawson, M. Esteban, H. Raghunathan, et al. “Bandwidth Studies of TE0n - TE0(n+1) Ripple-Wall Mode Converters in Circular Waveguide”.*IEEE Trans. Microwave Theory Tech.*,53 (1), 372-379 (2005).

[36] W. Lawson, M. R. Arjona, B. Hogan, et al. “The Design of Serpentine Mode Converters for High Power Microwave Applications”.*IEEE Trans. Microwave Theory Tech.*, 48, 809-814 (2000).

[37] I. Spassovsky, E. S. Gouveia, S. Tantawi, et al. “Design and Cold-Testing of a Compact TE_{01}-> TE_{20} Mode Converter”.*IEEE Trans. Plasma Sci*.,30, 787-793 (2002).

[38] www.ansys.com/Simulation/Software

[39] P. E. Latham, W. Lawson, and V. Irwin. “The Design of a 100 MW, Ku-Band Second Harmonic Gyroklystron Experiment”.*IEEE Trans. Plasma Sci*.,22, 804-817 (1994).

[40] G. P. Saraph, W. Lawson, M. Castle, et al. “100-150 MW Designs of Two and Three Cavity Gyroklystron Amplifiers Operating at Fundamental and Second Harmonics in X- and Ku-Band”.*IEEE Trans. Plasma Sci*.,24, 671-677 (1996).

[41] M. R. Arjona and W. Lawson. “Design of a 34 GHz Second-Harmonic Coaxial Gyroklystron Experiment for Accelerator Applications”.*IEEE Trans. Plasma Sci*.,28, 700-705 (2000).

[42] I. Yovchev, W. Lawson, G. S. Nusinovich, et al. “Present Status of a 17.1 GHz Four-Cavity Frequency-Doubling Coaxial Gyroklystron”.*IEEE Trans. Plasma Sci*.,28, 523-528 (2000).

[43] W. Lawson. “On the Frequency Scaling of Coaxial Gyroklystrons”.*IEEE Trans. Plasma Sci.*,30, 876-884 (2002)

[44] W. Lawson. “The Design of a High-Power, High-Gain, Frequency-Doubling Gyroklystron”. *IEEE Trans. Plasma Sci.*,33, 858-865 (2005).

[45] S. Tiwari and W. Lawson. “Design of a High-Gain K-Band Coaxial Gyroklystron”. *IEEE Trans. Plasma Sci.*, 35, 23-26 (2007).

[46] M. Veale, P. Purohit and W. Lawson. “Design of a High-Power, High-Gain, 2nd Harmonic, 22.848 GHz Gyroklystron”.*AIP Advances*, 3 , 082134 (2013).

[47] M. R. Arjona and W. Lawson. "Design of a 7 MW, 95 GHz, Three-Cavity Gyroklystron".*IEEE Trans. Plasma Sci.*, 27, 438-444 (1999).

[48] W. Lawson. "Design of a 70 GHz Second-Harmonic Gyroklystron Experiment for Radar Applications".*IEEE Microwave and Guided Wave Letters*, 10, 101-110 (2000).

[49] M. Walter, G. S. Nusinovich, W. Lawson, et al. "Design of a Frequency-Doubling, 35 GHz, 1 MW Gyroklystron".*IEEE Trans. Plasma Sci*.,28, 688-694 (2000).

[50] W. Lawson, R. L. Ives, M. Mizuhara, et al."Design of a 10 MW, 91.4 GHz Frequency-Doubling Gyroklystron for Advanced Accelerator Applications".*IEEE Trans. Plasma Sci*.,29, 545-558 (2001).

[51] P. E. Latham, W. Lawson, V. Irwin, et al. "High Power Operation of an X-Band Gyrotwistron". *Phys. Rev. Lett.*,72, 3730-3733 (1994).

[52] W. Lawson, P. E. Latham, J. P. Calame, et al. "High Power Operation of First and Second Harmonic Gyro-twystrons".*J. Appl. Phys*.,78, 550-559 (1995).

[53] G. S. Nusinovich, G. P. Saraph, and V. L. Granatstein. "Scaling Law for Ballistic Bunching in Multicavity Harmonic Gyroklystrons".*Phys. Rev. Letters*, 78, 1815-8 (1997).

[54] I. Yovchev, W. Lawson, M. Castle, et al. "Design of four-cavity high power gyroklystron amplifier". Proc. PAC-99, New York, 1999, 2, 1040-45.

[55] G. S. Nusinovich and H. Li. "Theory of the relativistic gyro-twystron".*Phys. Fluids B*, 4, 1058-65(1992).

[56] V. Ya. Davydovskii. "Possibility of resonance acceleration of charged particles by electromagnetic waves in a constant magnetic field".*Sov. Phys. JETP*, 16, 629 (1963).

[57] A. A. Kolomenskii and A. N. Lebedev. "Resonance effects associated with particle motion in a plane electromagnetic wave".*Sov. Phys. Dokl*., 7, 745 (1963).

[58] M. I. Petelin. "On the theory of ultra-relativistic cyclotron auto-resonance maser".*Radiophys. Quantum Electron*., 17, 686 (1974).

[59] V. L. Bratman, N. S. Ginzburg, G. S. Nusinovich, et al. "Relativistic gyrotrons and cyclotron autoresonance masers". *Int. J. Electronics*, 51, 541-568 (1981).

[60] G. S. Nusinovich, P. E. Latham, and O. Dumbrajs. "Theory of relativistic cyclotron resonance masers".*Phys. Rev. E*, 52, 998-1012 (1995).

[61] V. L. Ginzburg and I. M. Frank.*Dokl. Akad. Nauk SSSR*, 56, 583 (1947).

[62] C. S. Roberts and S. J. Buchsbaum. "Motion of a Charged Particle in a Constant Magnetic Field and a Transverse Electromagnetic Wave Propagating along the Field".*Phys. Rev.*, 135, 2A, 381 (1964).

[63] G. S. Nusinovich, P. E. Latham and H. Li. "Eficiency of Frequency Up-Shifted Gyrodevices: Cyclotron Harmonics Versus CARMs".*IEEE Trans. Plasma Sci*., 22, 796-803 (1994).

[64] P. E. Latham and G. S. Nusinovich. "Theory of relativistic gyro-traveling wave devices".*Phys. Plasmas*, 2, 3494-3510 (1995).

[65] P. E. Latham and G. S. Nusinovich. "Stability analysis of relativistic gyro-traveling wave devices".*Phys. Plasmas*, 2, 3511-3523 (1995).

[66] G. S. Nusinovich. "Cyclotron resonance masers with inhomogeneous external magnetic fields".*Phys. Fluids B*, 4, 1989-97 (1992).

[67] K. R. Chu, A. K. Ganguly, V. L. Granatstein, et al. "Theory of a slow wave cyclotron amplifier".*Int. J. Electronics*, 51, 493-502 (1981).

[68] G. S. Nusinovich, P. E. Latham, and S. Tantawi. "Cyclotron resonance masers with slow electromagnetic waves". 17^{th} Int. Conf. on IR&MM Waves, Dec. 1992, Pasadena, CA, USA, Conf. Digest, paper W4.5, 324-5 (1992).

[69] M. V. Nezlin. "Negative-energy waves and the anomalous Doppler effect".*Sov. Phys. Usp.*, 19, 946-954 (1976).

[70] N. S. Ginzburg."Nonlinear theory of amplification and generation of electromagnetic waves based on the anomalous Doppler effect".*Radiophys. Quantum Electron.*, 22, 323-9 (1979).

[71] S. Yu. Galuzo, V. I. Kanavets, A. I. Slepkov, et al. "Relativistic cyclotron accelerator exploiting the anomalous Doppler effect".*Sov. Phys. Tech. Phys*., 27, 1030-2 (1982).

[72] A. N. Didenko, A. R. Borisov, G. P. Fomenko, et al. "Cyclotron maser using the anomalous Doppler effect".*Sov. Lett. Phys. Lett*., 9, 572-3 (1982).

[73] G. S. Nusinovich, M. Korol, and E. Jerby. "Theory of the anomalous Doppler cyclotron resonance maser amplifier with tapered parameters".*Phys. Rev. E*, 59, 2311-21 (1999).

[74] G. S. Nusinovich, R. Ngogang, T. M. Antonsen, Jr., et al. "Overlapping of Resonances and Stochasticity of Electron Trajectories in Cyclotron Masers".*Phys. Rev. Lett*., 93, 055101 (2004).

[75] R. Ngogang, G. S. Nusinovich, T. M. Antonsen, Jr., et al. "Wave interaction in relativistic harmonic gyro-traveling-wave devices".*Phys. Rev. E*, 73, 056401 (2006).

[76] G. S. Nusinovich and J. Zhao. "Double resonance in cyclotron resonance masers".*Phys. Rev. E*, 58, 1002-10 (1998).

[77] J. P. Calame, J. Cheng, P. E. Latham, et al. "Amplification Studies of a Two-Cavity Second Harmonic Gyroklystron with a mixed-mode Output Cavity".*J. Appl. Phys.*75, 4721-4730 (1994).

[78] J. P. Calame, J. Cheng, B. Hogan, et al. "Measurements of Velocity Ratio in a 90 MW Gyroklystron Electron Beam".*IEEE Trans. Plasma Sci*.,22, 476-485 (1994).

[79] M. K. E. Flaherty, W. Lawson, B. Hogan, et al. "Operation of a K-Band Second Harmonic Coaxial Gyroklystron".*J. Appl. Phys.*76, 4393-4398 (1994).

[80] W. Lawson, B. Hogan, M. K. E. Flaherty, et al. "Design and Operation of a Two-Cavity 3rd Harmonic Ka-Band Gyroklystron".*Appl. Phys. Lett*.,69, 1849-1851 (1996).

[81] M. Castle, J. Anderson, W. Lawson, et al. "An Overmoded Coaxial Buncher Cavity for a 100 MW Gyroklystron".*IEEE Microwave and Guided Wave Letters*, 8, 302-304 (1998).

[82] X. Xu, C. Liu, J. Anderson, et al. "Development of an X-Band Advanced-Concept Input System for High-Power Gyroklystron".*IEEE Trans. Plasma Sci*., 27, 520-530 (1999).

[83] K. Bharathan, W. Lawson, J. Anderson, et al. "Design and Cold-Testing of a Radial Extraction Output Cavity for a Frequency-Doubling Gyroklystron".*IEEE Trans. Microwave Theory Tech.*, 38, 11, (2006). 1301- 1307 (2006).

[84] M. E. Read, W. Lawson, A. J. Dudas, et al. "Depressed Collectors for High Power Gyrotrons".*IEEE Trans. Electron Dev. Part* 2.,37, 1579-1589 (1990).

[85] G. P. Saraph, V. L. Granatstein, and W. Lawson. "Design of a Single-Stage Depressed Collector for High Power, Pulsed Gyroklystron Amplifiers".*IEEE Trans. Electron Dev.*,45, 986-990 (1998).

[86] M. Blank, B.G. Danly, B. Levush, et al."Experimental Demonstration of a W-Band Gyroklystron Amplifier".*Physical Review Letters*, 79, 4485-4488 (1997).

[87] M. Blank, B.G. Danly, B. Levush, et al."Demonstration of a 10 kW Average Power 94 GHz Gyroklystron Amplifier".*Physics of Plasmas*, 6, 4405-4409 (1999).

[88] B. Danly, M. Blank, J. P. Calame, et al. "Development and Testing of a High-Average Power, 94 GHz Gyroklystron".*IEEE Trans. Plasma Sci*.,28, 713-726 (2000).

[89] M. Blank, K. Felch, B.G. James, et al."Development and Demonstration of High Average Power W-Band Gyroamplifiers for Radar Applications".*IEEE Transactions on Plasma Science*, 30, 865-875 (2002).

[90] M. Blank, B.G. Danly, and B. Levush."Experimental demonstration of a W-Band (94 GHz) gyro-twystron amplifier". *IEEE Transactions on Plasma Science*, 27, 405-411 (1999)

[91] G.J. Linde, M.T. Ngo, B.G. Danly, et al."WARLOC: A High-Power Coherent 94 GHz Radar".*IEEE Transactions on Aerospace and Electronic Systems*, 44, 1102-1117 (2008).

[92] W.M. Manheimer, A.W. Fliflet, K. St Germain, et al."Initial Cloud Images with the NRL High Power 94 GHz WARLOC Radar".*Geophysical Research Letters*, 30, 1103 (2003).

[93] B. Levush, M. Blank, J. Calame, et al."Modeling and Design of Millimeter Wave Gyroklystrons".*Physics of Plasmas*, 6, 2233-2240 (1999).

[94] K.T. Nguyen, B. Levush, T.M. Antonsen, Jr., et al."Modeling of Gyroklystrons with MAGY".*IEEE Transactions on Plasma Science*, 28, 867-886 (2000).

[95] J.J Choi, A.H. McCurdy, F. Wood, et al. " Experimental Investigation of a High Power, Two Cavity, 35 GHz Gyroklystron Amplifier".*IEEE Transactions on Plasma Science*, 26, 416-425 (1998).

[96] J.P. Calame, M. Garven, J.J. Choi, et al. "Experimental Studies of Bandwidth and Power Production in a Three-Cavity, 35 GHz Gyroklystron Amplifier".*Physics of Plasmas*, 6, 285-297 (1999).

[97] M. Garven, J.P. Calame, K.T. Nguyen, et al. "Experimental Studies of a Four-Cavity, 35 GHz Gyroklystron Amplifier". *IEEE Transactions on Plasma Science*, 28, 672-680 (2000).

[98] K.T. Nguyen, J.P. Calame, D.E. Pershing, et al. "Design of a Ka-Band Gyro-TWT for Radar Applications".*IEEE Transactions on Electron Devices*, 48, 108-115 (2001).

[99] J.P. Calame, M. Garven, B.G. Danly, et al. "Gyrotron Traveling Wave Tube Circuits Based on Lossy Ceramics".*IEEE Transactions on Electron Devices*, 49, 1469-1477 (2002).

[100] M. Garven, J.P. Calame, B.G. Danly, et al. "A Gyrotron-Traveling-Wave-Tube Amplifier Experiment with a Ceramic Loaded Interaction Region".*IEEE Transactions on Plasma Science*, 30, 885-893 (2002).

[101] D.E. Pershing, K.T. Nguyen, J.P. Calame, et al. "A TE11 Ka-Band Gyro-TWT Amplifier with High-Average Power Compatible Distributed Loss".*IEEE Transactions on Plasma Science*, 32, 947-956 (2004).

[102] K.T. Nguyen, J.P. Calame, B.G. Danly, et al. "Higher Order Mode Excitations in Gyro-Amplifiers".*Physics of Plasmas*, 8, 2488-2494 (2001).

[103] A.S. Singh, S. Yuvaraj, and M. Thottappan."Analytical and PIC Simulation Studies of a Megawatt Class Gyro-twystron Amplifier".*IEEE Transactions on Electron Devices*, 63, 4104-4112 (2016).

[104] N. I. Zaitsev et al. "Experimental investigation of the relativistic mm-wave gyroklystron".*Radiophysics and Quantum Electronics*, 56, Nos. 8-9, 492-496 (2014).

[105] B. Hogan, W. Lawson, S. Tiwari, et al. "Operation of a four cavity, frequency-doubling gyroklystron".*2005 IEEE Int. Conf. Plasma Sci.*, Conference Record, 208,(2005)

[106] Sh. E. Tsimring. "Electron Beams and Microwave Vacuum Electronics". *Wiley-Interscience*(2007).

[107] N. F. Kovalev, I. M. Orlova, and M. I. Petelin. "Wave transformation in a multimode waveguide with corrugated walls".*Radiophysics and Quantum Electronics*, 11, 449-50 (1968).